Received: 22 March 2023 | Revised: 1 December 2023 | Accepted: 9 December 2023

DOI: 10.1002/jmor.21669

RESEARCH ARTICLE

JOURNAL OF morphology WILEY

Are owls technically capable of making a full head turn?

Aleksandra A. Panyutina[1] | Alexander N. Kuznetsov[2]

[1]School of Zoology, Faculty of Life Sciences, Tel-Aviv University, Tel Aviv, Israel

[2]Independent researcher, Israel

Correspondence
Aleksandra A. Panyutina, School of Zoology, Faculty of Life Sciences, Tel-Aviv University, Tel Aviv, 6997801, Israel.
Email: myotis@tauex.tau.ac.il

Abstract

The three-dimensional configuration of the neck that produces extreme head turn in owls was studied using the Joint Coordinate System. The limits of planar axial rotation (AR), lateral, and sagittal bending in each vertebral joint were measured. They are not extraordinary among birds, except probably for the extended ability for AR. The vertebral joint angles involved in the 360° head turn do not generally exceed the limits of planar mobility. Rotation in one plane does not expand the range of motion in the other, with one probable exception being extended dorsal bending in the middle of the neck. Therefore, the extreme 360° head turn can be presented as a simple combination of the three planar motions in the neck joints. Surprisingly, certain joints are always laterally bent or axially rotated to the opposite side than the head was turned. This allows keeping the anterior part of the neck parallel to the thoracic spine, which probably helps preserve the ability for peering head motions throughout the full head turn. The potential ability of one-joint muscles of the owl neck, the mm. intertransversarii, to ensure the 360° head turn was addressed. It was shown that the 360° head turn does not require these muscles to shorten beyond the known contraction limit of striated vertebrate muscles. Shortening by 50% or less is enough for the mm. intertransversarii in the middle neck region for the 360° head turn. This study has broad implications for further research on vertebral mobility and function in a variety of tetrapods, providing a new method for CT scan-based measurement of intervertebral angles.

KEYWORDS

aves, axial rotation, lateral bending, mm. intertransversarii, neck, range of motion, sagittal bending, vertebrate column

1 | INTRODUCTION

Neck mobility is crucial for birds since their forelimbs are engaged in flight. In fact, the avian neck plays the same role as the arm in humans. In this way, a chick uses neck motion for pecking seeds and a heron for harpooning a frog or fish. However, the reason for the evolution of extreme head mobility in owls (de Kok-Mercado et al., 2013; Krings et al., 2017; Steinbach & Money, 1973; Walls, 1963) was obviously different from this. It allows an owl to stay surreptitiously on a perch while looking around for prey and following it with its gaze if detected (Fux & Eilam, 2009). An ambush hunter needs to have a look at prey before attacking.

Live owls are known to turn their heads to either side in the horizontal plane for at least 270°, which is three-quarters of a full

turn (Steinbach & Money, 1973; Walls, 1963). Specific structural adaptations were found in owls that prevent damage to the neck nerves and blood vessels during extreme head turning (de Kok-Mercado et al., 2013). In experiments with a freshly deceased specimen of the tawny owl (*Strix aluco*), a full 360° turn of the head to either side was attainable without rupturing neck ligaments and muscles (Grytsyshina et al., 2016). Krings et al. (2017) reported that in the barn owl (*Tyto furcata*), the forced ex vivo turn of the head without rupturing ligaments and muscles was somewhat more than 360°, but they did not specify how much more, probably just a little. Also, owls are known to turn their heads in the vertical plane upside down to look all around something in front of them. Such head turns have not yet been studied at all, and the range of this motion is unknown. Can this turnover also reach 360° to every side or not, in cadavers at least?

1.1 | Previous studies of the neck motion involved in extreme head turn of owls

Grytsyshina et al. (2016) studied a fresh cadaver of the tawny owl in the skin; only feathers were removed. Based on CT scans, it was shown that the full 360° turn of the specimen's head was achieved through a combination of axial rotation (AR), lateral bending (LB), and sagittal bending (SB) in the neck joints. The numeric values of AR, LB, and SB angles were specified for 14 anterior joints. However, these values should be taken cautiously as a first rough approximation because of the low resolution of the CT scan used. It was not determined whether at least some of the joints could be rotated further and reach greater angles of AR, LB, or SB than observed in the 360°-turned specimen. Also, it was not considered whether, in each particular joint, the magnitudes of AR, LB, and SB in the case of the 360° turn are lower, equal, or higher than the limits of mobility available during planar AR, LB, and SB when only one degree of freedom (DoF) is employed in a joint.

Furthermore, one might inquire about whether the neck muscles are capable of turning an owl's head as much as a dead specimen allows. Doubts on this point were expressed by Krings et al. (2017), but the authors neither specified their concern nor suggested how to check this point. The authors examined head turning in fresh cadavers of the barn owl, with skin removed, but superficially, without CT-scanning, and did not present quantitative data on intervertebral mobility directly comparable to those of Grytsyshina et al. (2016). Also, Krings et al. (2017) studied in vivo head turning in barn owls for smaller angles of about 90° with X-ray fluoroscopy, but the insufficient resolution of the equipment did not allow the quantification of joint-specific rotations. Instead, quantitative data on attainable intervertebral angles were obtained by in silico modeling based on micro-CT scans of individual vertebrae. Thus, Krings et al. (2017) determined the angular limits for AR and LB in 15 anterior intervertebral joints of the barn owl by rotating virtual 3D models of vertebrae relative to each other. Based on the joint-specific AR and LB limits obtained in this way, they further attempted to reconstruct the maximum available cumulative angle of head turn with minimum deviations from the resting shape of the neck. SB was entirely excluded from the analysis of individual joints and was minimally involved in the reconstruction of the cumulative head turn, which was found to exceed 300°. Based on the data of Grytsyshina et al. (2016), such a large value seems doubtful without drawing the head into the shoulders by means of SB of the neck. An overestimate could come from the fact that the in silico modeling technique of Krings et al. (2017) did not take into account articular ligaments involved in the integrity of the natural joints. Also, the metrics for intervertebral angles were quite different in the two papers, as will be considered in detail in Section 2. On the whole, it is unlikely that the considerable quantitative discrepancies between the estimates of intervertebral AR and LB amplitudes by Grytsyshina et al. (2016) and Krings et al. (2017) are due to different species studied (*S. aluco* vs. *T. furcata*). Rather, they are due to quite different methods and metrics.

1.2 | Goal, hypotheses, and tasks

The goal of this research was to prove or disprove the existence of morpho-functional prerequisites in the owl neck for 360° head-turning performance, which has not yet been reported in live owls nor proved to be impossible. In this framework, the following hypotheses were posed:

1. A hypothesis that 360° is an approximate limit for head turn in all owls imposed by their shared geometry of intervertebral articulations and ligaments. If true, the maximal head turn could be expected to be ensured in different owl species by means of roughly similar neck configurations.
2. A hypothesis that, for the sake of increased head turning, owls possess a wider range of intervertebral mobility compared to other birds. If true, the next question is whether this is achieved through an excess mobilization in one or the other specific morphological plane or through facilitation of one motion by another in mixed motion.
3. A hypothesis that the 360° head turn of owls, if it is actually attainable in life, does not require an unusually large contraction range from neck muscles that would exceed the known properties of vertebrate striated muscles.

To test the hypotheses posed above, we solved the following tasks using fresh cadavers of a variety of owl species:

A. Quantification of available ranges of motion (aROMs) in every vertebral joint, when the motion is restricted to one specific anatomical plane. AR corresponds to motion in the transverse plane, LB to the frontal plane, and SB to the sagittal plane.
B. Quantification of the 360° head turn position in terms of used ranges of motion (uROMs) in every vertebral joint. For this purpose, intervertebral angles were decomposed into AR, LB, and SB. The interspecific diversity of the distribution of their magnitudes along the vertebral column was specified.

C. Sorting out the vertebral joints in which, during the 360° head turn, the limits of available planar mobility are undershot (uROM < aROM), matched (uROM ≈ aROM), or exceeded (uROM > aROM).
D. Measurement of contraction ranges required from one-joint neck muscles in the specimens with 360°-turned heads.

2 | MATERIALS AND METHODS

2.1 | Terminology

To designate the longitudinal polarity of the vertebral column, we will use the terms "cranial" and "caudal," as well as their synonyms "anterior" and "posterior," respectively. We will imply that the cranial end is the proximal attachment, and the caudal end is the distal attachment of the vertebral muscles. Thus, the anterior end of a muscle will be termed "the origin," and the posterior end will be termed "the insertion." In the same anteroposterior order, the vertebrae and the intervertebral joints are numbered. Roman numerals will be used for vertebrae. Thus, the atlas is number I. The first thoracic vertebra (T1), distinguished by bearing the first so-called "true" rib (i.e., the rib whose ventral segment reaches the sternum), is number XV in all owls studied (i.e., XV = T1). The first vertebra of the synsacrum (S1) is number XX (in *Strix* and *Surnia*) or XXI (in *Asio* and *Tyto*). The intervertebral joints will be numbered with Arabic numerals, with the number of a joint corresponding to the number of the vertebra located anterior to this joint. Thus, the occipital (cranium-atlas) joint is number 0. The atlas-epistropheus joint is number 1. The cervical-thoracic joint is number 14 in owls. The last intervertebral joint analyzed herein is number 18. Thus, the analyzed joints include the occipital one, 13 intracervical joints, cervical-thoracic one, plus four intrathoracic joints.

As for the movements, the following terminology is used. In every vertebral joint, including the occipital one, the relative position of the two articulated bones is decomposed into three components associated with the local anatomical planes. These components are axial rotation (AR), which is the movement in the transverse plane, lateral bending (LB) in the frontal plane, and sagittal bending (SB) in the sagittal plane. AR is also known as twisting. SB is often divided into flexion (movement in a ventral direction) and extension (movement in a dorsal direction). Krings et al. (2014, 2017) named AR "yawing," LB "rolling," and SB "pitching."

AR, LB, and SB components of intervertebral angles are assumed to be zero when the neck is perfectly straight. The planar AR, LB, and SB amplitudes, when only one degree of freedom (DoF) is employed for neck deviation from the straight position, can be named "planar available range of motion" or briefly "planar-aROM." The respective angles used in the 360° head turn can be named "360°-turn used range of motion" or briefly "360-uROM." Although the term "used range of motion" comes from the vocabulary of the studies of in vivo motions (the abbreviations uROM and aROM were introduced by Belyaev et al., 2021a), it is quite applicable to the 360° head turn of cadaveric (ex vivo) owls. Deviation from the straight position dorsalwards was assumed as positive SB, ventral-wards as negative SB. For AR and LB, a positive sign was assigned to deviations from the straight position in the same direction to which the head was turned, and a negative sign was assigned to opposite deviations. Note that we will present angular deviations from the straight position to one side or the other, not from side to side. Therefore, our values should be doubled for comparison with side-to-side measurements provided in some other publications (e.g., Belyaev et al., 2021a, 2021b, 2022; Kambic et al., 2017).

2.2 | Animals

The material comes from collections of the Zoological Museum of Lomonosov Moscow State University and A.N. Severtsov Institute of Ecology and Evolution, Russian Academy of Sciences. The fresh cadavers were stored frozen in feathers and thawed immediately before being studied. Eight individuals of five species from four genera of owls (Table 1) were studied, namely: three specimens of short-eared owl *Asio flammeus* (Pontoppidan, 1763), one specimen of Ural owl *Strix uralensis* Pallas, 1771, two specimen of tawny owl *S. aluco* Linnaeus, 1758, and one specimen each of northern hawk-owl *Surnia ulula* (Linnaeus, 1758), and barn owl *Tyto alba* (Scopoli, 1769). All individuals were adults except one of the two *S. aluco* specimens, which was juvenile. In the specimen *A. flammeus* #2, posterior thoracic joints were not studied because of trauma in this place (at the XVIII-th vertebra), which probably led to the owl's death in a road accident. For a similar reason, in the specimen of *S. uralensis*, the skull was somewhat damaged, but it did not touch the occipital region involved in our analysis.

2.3 | Postures

A frozen cadaver specimen was thawed, drawn in one of the required postures, and packed in this position in the scanning holder; in some cases, it was frozen in the holder again before CT scanning. In one specimen of *A. flammeus* (#1), the skin and the shoulder girdle with musculature were removed before scanning. All other specimens were scanned without the removal of feathers or any body parts.

Six postures were probed for intervertebral angles. (1) 360° head turn for measuring 360-uROMs; (2) straight vertebral column for measuring the "neutral" SB angles; (3) straight vertebral column maximally twisted to one side for measuring AR planar-aROMs; (4) neck maximally bent to one side in the frontal plane for measuring LB planar-aROMs; (5, 6) neck maximally bent dorsally or ventrally in the sagittal plane for measuring SB planar-aROMs. In the case of probing the 360° head turn (posture 1), we took care of the head position, making it face as much as possible like in the resting position of an owl sitting on a perch, but did not care about the neck, allowing it to freely coil by itself and draw the head into the shoulders. In the straight untwisted posture (2), the vertebral column was kept as straight as possible, and the head was placed like when probing 360-uROMs, so as to face forward. In postures

TABLE 1 Joints which angles were quantified in different owl specimens and postures.

Specimens (*N* = 8)	360° Turn	Direction	Straight	Straight twisted	Direction	Bent laterally	Direction	Bent dorsally	Bent ventrally
Asio flammeus #1			0–18	0–18	Right	0–18	Right	0–18	0–18
A. flammeus #2	0–15*	Right	0–15	0–15	Right	0–15, 0–13	Right	0–15, 5–15	
A. flammeus #3	0–18*	Right							
Strix uralensis	0–18*	Right							
Strix aluco ad	0–18*	Left	0–18	0–18	Right				
S. aluco juv	0–18*	Left							
Surnia ulula	0–18*	Left		0–18	Right				
Tyto alba	0–18*	Left	0–17						

Note: Number 0 is the occipital joint, number 18 is the joint between vertebrae XVIII and XIX which is in owls, the 4-th intrathoracic joint. The one specimen of *A. Flammeus* (#1) was CT-scanned after removal of the shoulder girdle. The specimens which neck muscles were dissected after CT scanning are indicated in bold. *postures for which muscle length analysis was done.

3–6, required to measure planar-aROMs, we paid primary attention to the position of the neck, which had to be maximally rotated in the respective direction in each intervertebral as well as the occipital joint but remain straight in other directions.

In total, 23 CT scans were studied. All specimens (*N* = 8) except one were examined with the 360° head turn (*N* = 7). *Surnia*, *S. aluco*, and two specimens of *A. flammeus* (*N* = 4) were also CT-scanned with the maximally twisted but straightened vertebral column to quantify the planar AR aROM. *T. alba*, *S. aluco*, and two specimens of *A. flammeus* (*N* = 4) were studied with an untwisted straightened vertebral column to measure the "neutral" SB angles in the intervertebral joints. The same two specimens of *A. flammeus* (*N* = 2) were CT-scanned with the vertebral column maximally bent to one side to quantify the planar LB aROM (three scans), and with the vertebral column maximally bent ventrally (one scan) and dorsally (three scans) to quantify the planar SB aROM. Overall, six different postures were probed in *A. flammeus*, which is thus our central model species.

In the straightened specimens, we were unable to ensure perfect straightness of the vertebral column, especially at the neck–thorax transition. Therefore, to obtain the "neutral" SB angles, we averaged the respective joint-specific values in the four specimens studied in the straightened posture. It was inadequate to use a similar averaging procedure for the straight-twisted as well as laterally and sagittally bent specimens because it was impossible to reach the limit of respective movement in all joints of a single specimen simultaneously. In each specimen, only some joints reached the limit of available mobility, and those joints were different in different specimens. Therefore, for each joint, we selected the maximal angle found among the tested specimens for the final analysis of planar AR, LB, and SB aROMs.

2.4 | CT scans processing

CT scanning was performed with the CT Phoenix V|tome|x m 300. The obtained raw projection data from the scanner (back projections) were converted into a volume using the software shipped with the Phoenix V|tome|x scanner (Phoenix datos|x). Then, series of cross-section images (slices) were exported from the volume and saved in DICOM format. The series included from 1500 to 2200 slices per scanned specimen. The series were processed with Slicer 4.10 software as follows: The grayscale threshold was set to match the X-ray density of the specimen's skeleton. The holder of the specimen was manually cut out, along with unnecessary parts of the specimen, such as the wings and shoulder girdle, trachea, anterior part of the skull, and hindquarters. The removed parts not only masked the vertebral column but also wasted computer power. The necessary parts, including the vertebral column up to the pelvis and the posterior part of the skull, were converted to a vector model in STL format for further processing (the examples of STL models presented in Files S1 and S2 retain unnecessary parts of the skeleton to facilitate anatomical referencing). In some specimens, the X-ray density considerably varied along the vertebral column, requiring separate processing of its parts and creation of a composite vector model. The points required for the analysis of neck geometry (up to 82 points in the case of 19 analyzed joints, FCSV files in Files S1 and S2) and for the analysis of lengths of selected muscles (44 points) were placed on the vector model with the Markups tool of Slicer 4.10 (MRML files in Files S1 and S2). For vertebrae, the points were placed on the apices of the left and the right prezygapophyses and postzygapophyses. For the occipital joint, the "postzygapophysial" points R_0 and L_0 were placed on the skull at the sides of the occipital condyle. An additional pair of anterior-most points required for the decomposition of the occipital joint angle was placed on the inner surface of the os basioccipitale at the foramina n. hypoglossi. Finally, x, y, and z coordinates of all the marked points were exported from Slicer 4.10 via a CSV-format file into specially arranged templates of MS Excel 2003/2007 for quantitative analysis (File S3).

2.5 | Analysis of neck geometry

Decomposition of intervertebral rotation into three components is not a simple task. Krings et al. (2017) in their in silico simulations of owl's neck mobility follow Euler's method. In every pair of successive vertebrae, they describe the position of the posterior one as rotations in the Cartesian coordinate system fixed to the anterior one. The origin of the coordinate system is placed in the center of a virtual sphere inscribed into the posterior articular surface of the anterior vertebra. The longitudinal and the vertical axes of the anterior vertebra passing through this center are treated, respectively, as the axes of AR ("yawing") and LB ("rolling") for the posterior vertebra. The transverse axis of SB ("pitching") was attached by Krings et al. (2017) not to the posterior articular surface of the anterior vertebra but to the anterior articular surface of the posterior vertebra in a pair. This is reasonable because the intervertebral joints of the avian neck are saddle-shaped (heterocoelous) and, hence, cannot be approximated by a single sphere as a ball-and-socket joint. This complication was probably one of the reasons why Krings et al. (2017) omitted the analysis of SB in owl's neck. Two sets of simulations were developed by Krings et al. (2017): AR-first, and LB-first. One was used to obtain the extreme AR with the subsidiary help of LB, and the other was used to obtain the extreme LB with the subsidiary help of AR. It should be noted that the fundamental feature of Euler's method is the importance of the order of elementary rotations. The same resultant position of the body in 3D space is achieved with different angles of rotation around the fixed orthogonal axes depending on the order in which these rotations are applied.

An alternative method of rotation decomposition was applied by Kambic et al. (2017) to the turkey's neck. Instead of Euler's method with the Cartesian coordinate system fixed to one of the two vertebrae, they used the so-called "joint coordinate system" (JCS). One of the three axes is fixed to the anterior vertebra, the other to the posterior vertebra, and the third one is floating and is built as a common perpendicular to the former two. Those two fixed axes are not necessarily orthogonal to each other, and hence the whole JCS is not a Cartesian one. First, the JCS methodology was developed by Grood and Suntay (1983) for the human knee joint. Two advantages of this method were announced. The first was that in this decomposition of 3D rotation, the values of the three elementary rotations (i.e., the rotations about the two fixed and one floating axis) do not depend on the order in which they are applied. However, this is not completely true. In fact, the decomposition result depends now not on the order of rotations but on the solution of which particular axes are fixed to the two articulated bodies (bones), and which one is left to float as their common perpendicular. The second advantage is the better correspondence of the JCS axes to those traditionally used in anatomy. For instance, in the knee, flexion-extension (analogous to SB in the vertebral column) is traditionally measured relative to the transverse axis of the femoral condyles, but AR (pronation and supination) is measured relative to the longitudinal axis of the shank. For comparison, in the Cartesian coordinate system with all three axes fixed to the femur, the AR of the shank about its own longitudinal axis always undergoes decomposition that depends on the knee flexion angle. The traditional relation of the flexion-extension axis to the femur and of the AR axis to the tibia was kept by Grood and Suntay (1983) in the knee JCS, which they invented. They made the axis of abduction-adduction (analogous to LB in the vertebral column) a floating axis as this motion is of minor importance in the human knee. Later, it was proposed to extend the JCS methodology as a biomechanical standard for all human joints (Wu et al., 2002, 2005). For the intervertebral joints, Wu et al. (2002) strictly followed the approach of Grood and Suntay (1983) to the knee: the transverse axis of SB was fixed to the proximal (anterior) vertebra in a pair, the longitudinal axis of AR was fixed to the posterior (distal) one, and the dorsoventral axis of LB was made the floating axis. Kambic et al. (2017) used for the turkey the opposite variant: LB axis was also chosen as the floating one, but the AR axis was fixed to the anterior vertebra, and the SB axis was fixed to the posterior vertebra (it is not written in the paper but was personally clarified by Dr. Kambic via ResearchGate). In case of the intervertebral joints, there is no such tradition as with the knee and other limb joints, which favors association of the AR axis with the anterior or posterior vertebra. The saddle-shaped structure of the avian neck joints favors fixation of the LB axis to the anterior vertebra and the SB axis to the posterior vertebra, thus leaving the AR axis as the floating one. Formally, six combinations of the JCS axes are possible. Listing the axes in the order (proximal fixed)-(floating)-(distal fixed), these combinations are SB-LB-AR, AR-LB-SB, LB-AR-SB, SB-AR-LB, AR-SB-LB, LB-SB-AR. They produce somewhat different decompositions of joint positions.

In addition to Euler's method and the JCS method, both of which treat the vertebral column as a chain of rigid bodies, a third approach was applied to the vertebral column mobility by Grytsyshina et al. (2016). Its idea is the approximation of the vertebral column with a flexible rod. Imagine a straight rubber rod with two longitudinal lines L (left) and R (right) drawn on its surface. Each line is marked with a series of points making bilaterally symmetrical pairs on the left and right sides of the rod. The part of the rod from one point pair to the next is treated as the rod segment. When the rod is deformed, the coordinates of the points can be used to quantify intersegment deformations.

It should be noted that the flexible rod model provides anatomically consistent decomposition of intervertebral rotations, similarly to the JCS developed by Grood and Suntay (1983) and applied to the avian neck by Kambic et al. (2017). The flexible rod model has certain advantages compared to the JCS model treating the backbone as a chain of rigid segments. To characterize the position of vertebra as a rigid body in 3D space, three points at least are necessary to be specified on it. Kambic et al. (2017) marked vertebrae with four points. Two of them were placed on the apices of the left and right prezygapophyses, and the other two were placed at the anterior and posterior ends of the floor of the neural canal. For the method of Grytsyshina et al. (2016), only two points per segment were enough. The poor quality of the CT scan did not allow Grytsyshina et al. (2016) to locate the apices of prezygapophyses or

postzygapophyses. Instead, the markers were placed at the midpoint of each postzygapophysis-prezygapophysis contact. These contacts could be located well enough even in a poor-quality CT scan.

In the current research, we decomposed intervertebral angles using JCS methodology (Kambic et al., 2017; Wu et al., 2002). Our calculations were based on Cartesian coordinates of the apices of prezygapophyses and postzygapophyses, that is, two pairs of points per vertebra (Figure 1a). These apices are advantageous landmarks because they are not only very well-visible on 3D models but also because they are located far apart from each other, thus providing a reliable basis for precise geometric calculations. The line connecting the apices of the left and the right zygapophyses in a pair has a transverse orientation in the body. Thus, it is parallel to the rotational axis of SB and can be used as a replacement of this axis in SB angle calculations, whether the true axis coincides with this line or only parallels it. Similarly, when calculating AR angle, any longitudinal line in a vertebra can be used as a geometric replacement for the true rotational axis of AR. In our metric, it is the line through the midpoints of the two transverse segments—one bridging the apices of the left and the right prezygapophyses, the other one bridging the apices of the left and the right postzygapophyses of the same vertebra (Figure 1c). Following Wu et al. (2002), in a joint number n, the SB axis should be fixed to the preceding vertebra (number N), and in our metric, it would be represented by the line connecting the apical points of its left (L_n) and right (R_n) postzygapophyses (Figure 1d). The AR axis should be fixed to the next vertebra (number N+1), and in our metric, it would be represented by the line connecting the midpoint (m_n) between its prezygapophyses and the midpoint (M_{n+1}) between its postzygapophysis. The common perpendicular to those two axes, one fixed to the N-th and the other to (N+1)-th vertebra, would be the rotational axis of LB, which is not fixed to any vertebra but is a floating axis of this JCS. Following Kambic et al. (2017), the order of fixed axes would be reverse: for the same joint number *n*, the AR axis should be fixed to the N-th vertebra, while the SB axis to the (N+1)-th vertebra. In our metric, these axes would be represented, respectively, by the longitudinal line ($m_{n-1}M_n$) of the former, and the interprezygapophysial transverse line (l_nr_n) of the latter (Figure 1e). The common perpendicular to those two lines would be the rotational axis of LB, and it is the floating axis again. We used both variants of JCS for intervertebral angle decomposition and present here the averaged values of the two (original values for each JCS can be found in tables in File S3). It is worth noting that three points are enough to specify the position of a rigid body in 3D space by its characteristic plane or triangle. We had four points per vertebra and four points for the skull. In every calculation, four points were reduced to three ones by

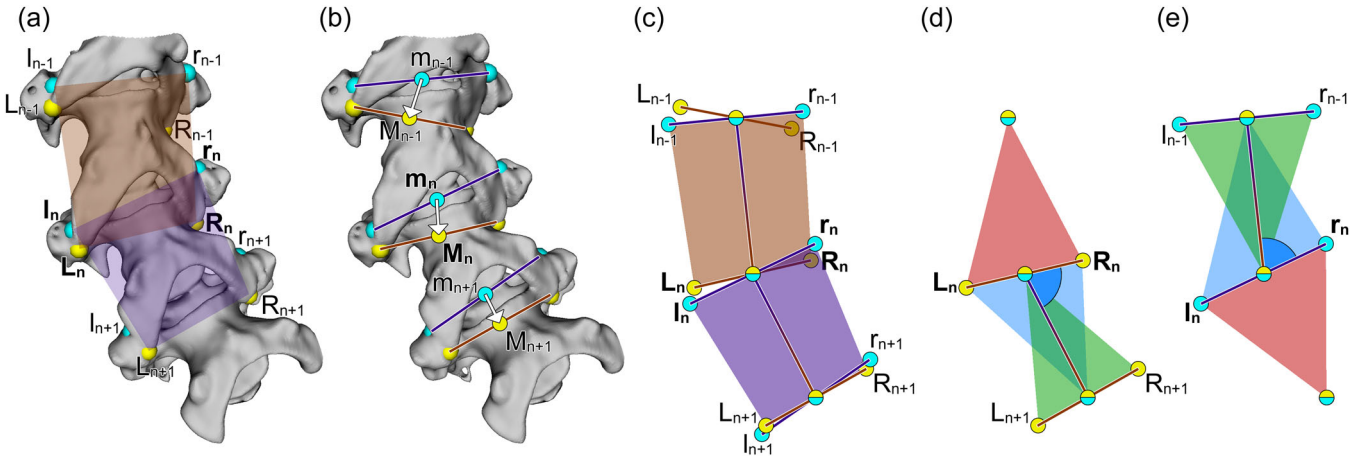

FIGURE 1 CT-scan-based method of decomposition of an intervertebral angle into axial rotation (AR), lateral bending (LB), and sagittal bending (SB) components using Joint Coordinate System (JCS); joint number **n** as an example. (a) Dorsal view of part of the owl neck skeleton with markup of zygapophysial apices in three successive joints (n−1, **n**, and n+1); postzygapophyses are marked with yellow balls and labeled with uppercase letters, prezygapophyses—with cyan balls and lowercase letters; l/L—left zygapophyses, r/R—right ones; vertebra number N is specified by the brown quadrangle [$l_{n-1}r_{n-1}\mathbf{R_nL_n}$], vertebra number N+1—by the violet quadrangle [$\mathbf{l_nr_n}R_{n+1}L_{n+1}$]. (b) Finding geometric midpoints for each pair of prezygapophyses (cyan dots) and postzygapophyses (yellow dots). (c) A midline is built for each vertebra which connects its mid-prezygapophysial and mid-postzygapophysial points, and the vertebrae are translated (but not rotated) relative to each other so that, in each joint, the mid-postzygapophysial point of anterior vertebra coincides with the mid-prezygapophysial point of the next one (these translations are shown in (b) by white arrows). (d) JCS of the joint **n** following Wu et al. (2002); SB rotational axis (**L_nR_n**) belongs to the N-th vertebra which plane is specified by the red triangle; AR axis is the midline of the (N+1)-th vertebra which plane is specified by the green triangle; LB angle is measured between those two axes in their common plane represented by the blue triangle; SB angle is the angle between the red and the blue planes; AR angle is the angle between the green and the blue planes. (e) JCS of the same joint **n** following Kambic et al. (2017); AR axis is the midline of the N-th vertebra which plane is specified by the green triangle; SB rotational axis (**l_nr_n**) belongs to the (N+1)-th vertebra which plane is specified by the red triangle; LB angle is measured between those two axes in their common plane represented by the blue triangle; SB angle is the angle between the red and the blue planes; AR angle is the angle between the green and the blue planes.

replacing one or the other pair of zygapophysial points with their respective midpoint (Figure 1).

It should be emphasized that we did not calculate translations. This allowed us to avoid searching for the true morphological locations of the fixed rotational axes and directly use the zygapophyses-based lines—(L_nR_n) and (m_nM_{n+1}) in the first JCS variant, and ($m_{n-1}M_n$) and (l_nr_n) in the second variant. A trick for simpler calculation of angle decomposition was a virtual translation (translation does not affect angular dimensions) of the posterior vertebra in a pair so that its interprezygapophysial midpoint m_n exactly coincides with the interpostzygapophysial point M_n of the preceding vertebra (Figure 1b,c). This point thus becomes the origin of coordinates for both JCS variants where all their axes intersect (Figure 1d,e).

In the case of AR and LB, deviations to the right and the left sides can be easily sorted out due to bilateral symmetry of these movements relative to the sagittal plane. In the case of SB, there is no such plane of symmetry, and distinction between flexion to the ventral side and extension to the dorsal side depends on convention about the zero position. We assume it to be the straight position. However, the zygapophyses-based metric does not provide the straight position immediately but requires an additional correction. This is because the apices of zygapophyses, due to their different heights, do not form a straight line in the sagittal plane when the vertebral column is perfectly straight. To overcome this discrepancy, we have applied the following procedure to *A. flammeus* (two specimens), *S. aluco*, and *T. alba* with the straightened untwisted vertebral column (Table 1). First, we obtained joint-specific SB angles for each straightened specimen based on prezygapophyses' and postzygapophyses' markups. Then we averaged the prezygapophyses-based and postzygapophyses-based values for each specimen. Finally, we averaged the joint-specific values of all four straightened specimens. The resultant SB angles were used as the angular profile of the straight vertebral column. For all other specimens, turned, twisted, and bent, this profile was used to distinguish between the ventral flexion and the dorsal extension. Technically, the "raw" SB angles obtained for each specimen as described above were converted to the "net" SB angles by subtraction of the SB angles of respective joints in the straightened specimens.

2.6 | Analysis of muscle lengths

Shortening range of sarcomeres in striated muscle has been shown to be predictable from musculoskeletal geometry (e.g., Dimery, 1985; Weijs & van der Wielen-Drent, 1983). This provides a firm basis for our approach to muscle length treatment.

After CT scanning, the neck muscles were dissected in the specimens of *A. flammeus* #1 and *S. ulula*. For quantitative analysis, the mm. intertransversarii were selected since they are one-joint muscles, and hence, their fiber lengths are expected to be more directly correlated with the vertebral joints' aROMs than in other neck muscles operating more than one joint. The mm. intertransversarii operating on seven intervertebral joints, from the fourth to the 10th, were dissected in detail. They were separated into portions, and for each portion of each joint, the midpoints of origin and insertion were located on the skeleton. Then, the same points (44 on both sides) were marked with Slicer 4.10 software on the vector models of the 360°-turned specimens of not only *A. flammeus* and *S. ulula*, which were dissected, but also of five other specimens (Table 1). Having exported x, y, and z coordinates of all 44 points from Slicer to MS Excel, we calculated the lengths of the muscular portions, which were selected, as the straight distances from the point of origin to the point of insertion (Figure 2). Approximation of short one-joint muscles with a straight line without taking into account the curvature of the neck surface is quite reasonable.

The next assumption was that the length of the muscular belly is approximately equal to the fiber length. This is based on the fact found during our dissection that aponeuroses in the mm. intertransversarii of owls are much reduced compared to the typical avian condition (Landolt & Zweers, 1985; Zusi & Storer, 1969). Thus, for each 360°-turned specimen, we obtained the lengths of each muscular portion under study on the left and the right sides. The difference between the two lengths divided by the larger one and represented in percentages was taken as the measure of the relative shortening range required from this muscular portion for achieving the 360° head turn. These percentages were compared in different portions, joints, and specimens.

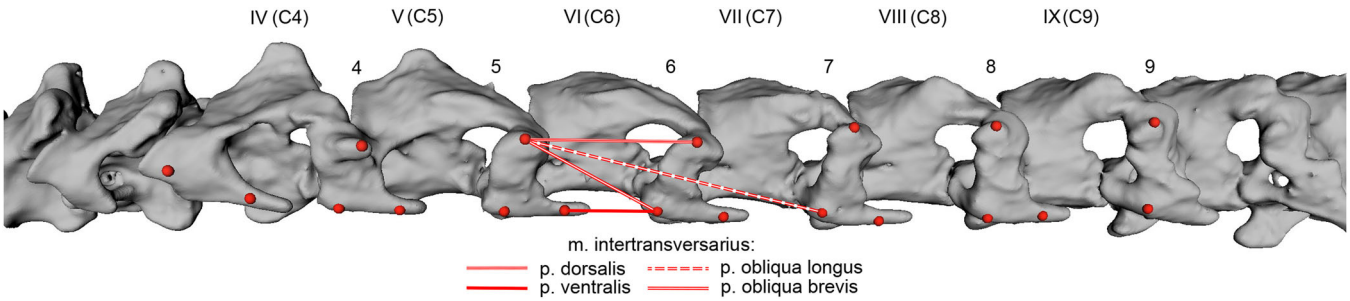

FIGURE 2 Diagram of the major attachment points of portions of mm. intertransversarii in the middle of owl's neck. Lateral view from the left side. Lines of actions of all four portions are shown for the m. intertransversarius of joint 6. An unusual two-segment p. obliqua longus was not included in the muscle length analysis.

2.7 | Limitations

Unfortunately, we CT-scanned the *A. flammeus* #1 (Table 1) after removing the skin, wings, and shoulder girdle. We did this for better visual control of the neck position in the postures bent laterally, dorsally, and ventrally. This was done at the beginning of our research, and we did not expect a negative result of this dissection. It appeared that the removal of the shoulder girdle gives additional freedom to deviations of the neck base, which resulted in rather unusual intervertebral angles along the neck in the 360°-turned posture of this specimen. Therefore, it was excluded from the analysis of the 360° head turn and was only involved in analyses of the ranges of planar motions.

We were unable to ensure a perfectly equal pitching angle of the head in 360°-turned, straight-necked, straight-twisted, and laterally bent specimens. As a result, the SB angle in the joint number 0 is not representative enough in our study. However, it is least important for achievement of the 360° head turn.

We are not sure that we reached the limits of planar bending (LB, and the dorsal and ventral directions of SB) in all joints of the specimens studied in respective postures (Table 1). The main problem is the large flexibility combined with the large head of owls. Thus, bending the neck in each direction soon results in the meeting of the head and trunk. Therefore, we could not bend the neck to the true extreme and somewhat underestimated the planar bending aROMs in some joints. For a future researcher who will not be confined by CT-scanning time as we were, we would recommend making from six to nine scans per bending direction to ensure maximal bending of two or three joints in one scan, the next two or three in the other, and so on.

Compared to LB and SB, it was easier to reach the limits of planar AR (straight twisted specimens). However, even in this motion, there remained some uncertainty in the caudal-most cervical and thoracic joints. Thus, there was found a −2° AR angle in the opposite direction to the general neck twist and head turn in the 13th (last cervical) joint in the *A. flammeus* #2 straight-twisted specimen and in the 18th (last studied) joint of the *S. ulula* straight-twisted specimen.

The data supporting the findings of this study are available in the supplementary material to this article. The original CT scans are uploaded to the morphosource.org repository https://www.morphosource.org/projects/000549076/ and available on request.

3 | RESULTS

In all owl species studied, fresh specimens allowed for a full head turn of 360° (720° in both directions) without any harm to the ligaments and muscles of the neck. The 360° turns were easily achievable, provided that the head was allowed to retract freely into the shoulders (Figure 3). This retraction is driven by the coiling of the neck, which occurs automatically when an experimenter turns the specimen's head, much like a rope shortens and coils with twisting. At 360° or slightly more, the head's turn is halted by internal tension in the specimen, most likely in the intervertebral ligaments. Interestingly, after yawing the head by 360° in the horizontal plane, it can be returned to the resting position by rolling it in the vertical plane

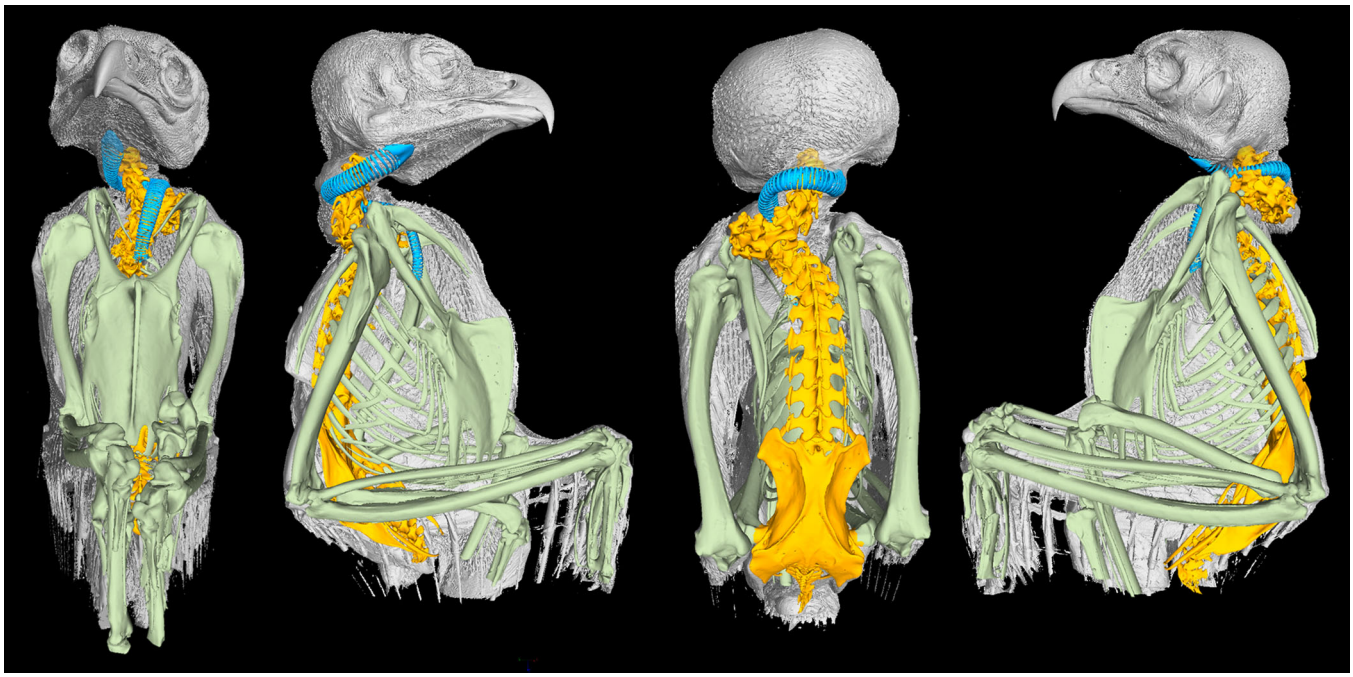

FIGURE 3 CT-scan set demonstrating the 360° head turn to the left side in the fresh dead specimen of *Surnia ulula*. From left to right: front side view, right side view, back side view, and left side view. Orange—backbone and pelvis; blue—trachea; pale green—ribs, shoulder girdle, fore and hind limbs; gray—skin surface under plumage.

(File S4). The reverse order, rolling to 360° and yawing back to 0°, is equally feasible. Thus, there is an equifinality at the 360°-turned head position, which is the same after a full turn in either of the two planes.

3.1 | Axial rotation

3.1.1 | Axial rotation with straight neck: AR planar-aROM

Four specimens were studied with straight and maximally twisted vertebral columns (Table 1, Figure 4a). The cumulative AR planar-aROM across 19 studied joints in three specimens varied from 122° to 182° (Table S5).

Taking, for every joint, the maximum value found across studied specimens, the AR planar-aROM profile was built. It showed a general decrease of joint-specific values in the caudal direction (Figure 4a). The largest AR planar-aROM value of 40° was found in the occipital joint. In joint 1, the value was 30°. In joints 2–6, the values still exceeded 10° with the local minimum of 10° in the fourth joint. In joint 7, the value dropped to 10° again. Starting from joint 8, the values were below 10°.

3.1.2 | Axial rotation with full head turn: AR 360-uROM

The distribution of AR in the 360°-turned specimens was as follows (Figure 5a). The largest AR 360-uROM was found in the occipital joint (Table S5; Figure 5a). Within the neck, AR was most pronounced in joints 1–3, 5 and 6. In contrast, AR was almost absent in the fourth joint. Joints 8–13 were either rotated in the opposite direction to the head turn or remained nonrotated. The distribution of AR along the vertebral column with the 360° head turn can be summarized as follows: Joints 0 and 1 had large positive AR, joints 2 and 3 had modest positive AR, joint 4 had almost zero AR, joints 5–7 had modest positive AR, joints 8–13 had negative or zero AR, and joints 14–18 had positive or negative AR of small magnitude.

It was unexpected that in the 360°-turned specimens, AR in some joints could occur in the opposite direction to that of the head turn. Joints 8–13 were twisted to the "negative" side in all studied specimens. Joints 14–18 had AR 360-uROMs that varied near zero in both directions. The overall contribution of vertebral AR to the 360° head turn, obtained by simply summing the joint-specific AR values for all 19 joints studied, ranged from only 56° in *S. uralensis* to 126° in *A. flammeus* #3. However, to estimate the actual involvement of vertebral AR in the 360° head turn, the twist directions in individual joints should be disregarded, and the absolute joint-specific magnitudes of AR 360-uROMs summed up. This sum ranged from 102° in *T. alba* to 158° in *A. flammeus* #3 (Table S5; these sums are visualized by the total heights of bars in Figure 5b).

Among the seven specimens studied with the 360° head turn, the difference between the maximum and minimum values of AR 360-uROMs in the occipital joint was 23° (Figure 5c). The respective differences for intervertebral joints spanned from 2° to 14°. The greatest difference was found in joints 1–3, and the smallest difference was in joint 13 (the last intracervical joint) and 16. On the whole, the most uniform AR 360-uROMs were found in joints with modest positive or close-to-zero mean values, while the least uniform joints were those with the largest mean values of AR 360-uROM.

3.2 | Lateral bending

3.2.1 | Bending in the frontal plane: LB planar-aROM

Two specimens of *A. flammeus* were studied with the neck bent to the side in the frontal plane; one of the specimens was laterally bent and CT-scanned in this position two times. Taking, for each joint, the greatest absolute value achieved in the three scans, the maximal available cumulative LB of 299° was obtained for all 19 joints together (Table S5; Figure 4b). The LB planar-aROM showed an uneven distribution along the vertebral column. The joint-specific LB planar-aROMs were highest in joints 0, 2, 3 and 8–14, intermediate in joints 1, 4–7, and lowest in joints 15–18. The LB planar-aROM found in the cervical-thoracic joint is a very high value indeed. It is approximately as high as in the preceding intracervical joints in the caudal part of the neck, while in the following intrathoracic joints, the joint-specific values are the lowest in the vertebral column.

3.2.2 | Lateral bending with full head turn: LB 360-uROM

The distribution of LB in the 360°-turned specimens was as follows (Figure 5d). Joints 0–3 were bent in the direction of the head turn; the only exception was *T. alba*, showing a slight opposite (negative) bend in joints 2 and 3. Starting with joint number 4, the LB direction changed to negative in all specimens. Beginning with joint 8 or 9 (in *T. alba*), the LB direction again corresponded to the head turn direction. It remained positive in the caudal intracervical joints 9–13. At the cervical-thoracic joint, the LB 360-uROM magnitude decreased. In the four cranial intrathoracic joints (15–18), the LB 360-uROMs varied around zero.

For all 19 joints together, the sum of joint-specific LB 360-uROM absolute magnitudes (disregarding bend direction) ranged from 136° in *T. alba* to 204° in *A. flammeus* #3 (Table S5; these sums are visualized by the total heights of bars in Figure 5e).

Like in the case of AR, some joints showed the opposite direction of LB relative to the direction of the 360° head turn. The sum of LB 360-uROMs in those joints which were bent to the same side as the

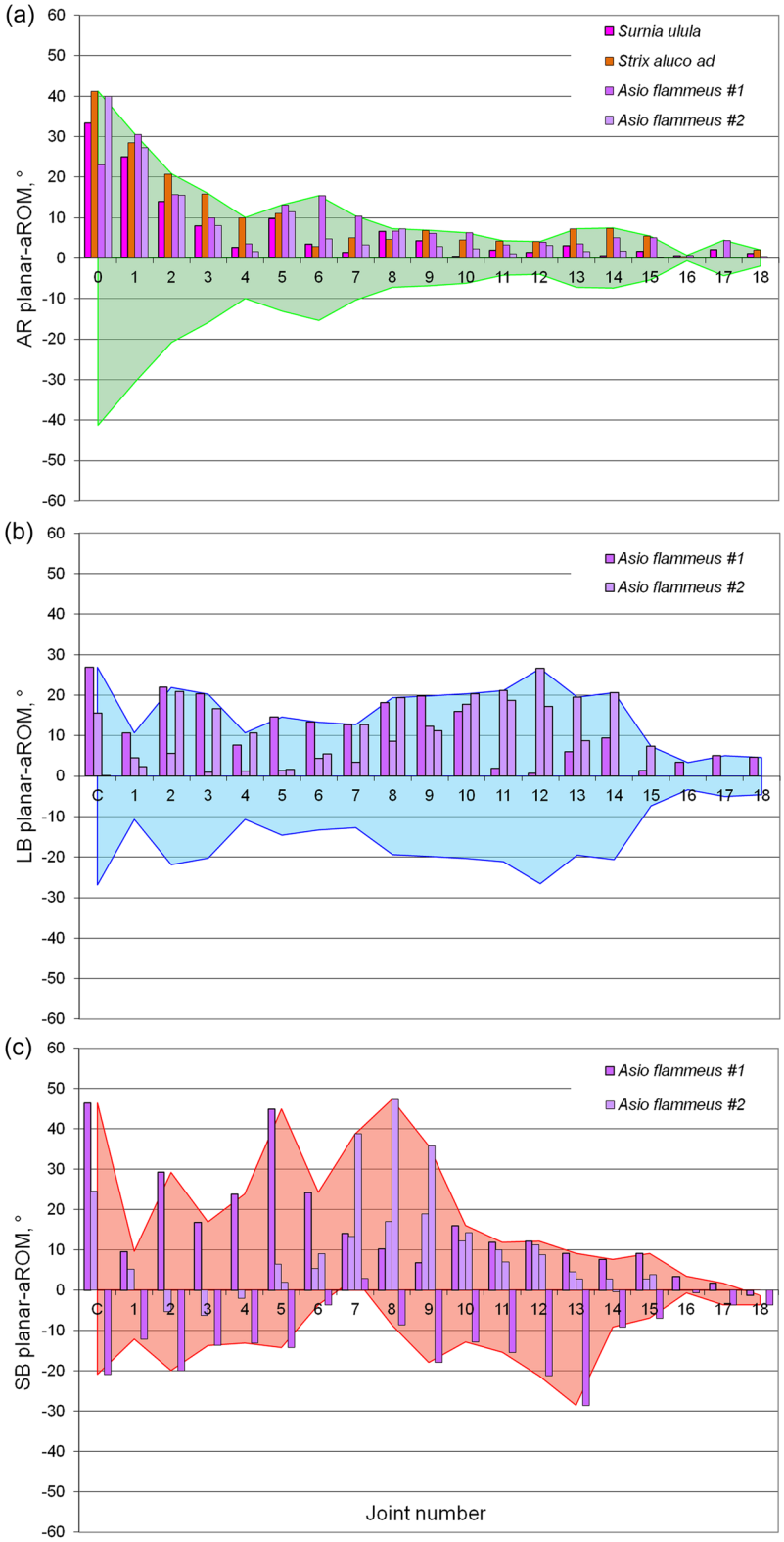

FIGURE 4 The limits of planar mobility in the vertebral joints of owls relative to the straight posture represented by the abscissa axis. (a) axial rotation, (b) lateral bending, (c) sagittal bending. In each direction, the full range of motion from side to side is represented by the vertical distance between the upper and the lower boundary lines of the respective plot. In (a) and (b), the full range is obtained by mirroring the boundary line across the abscissa axis. The bars represent the data obtained from particular specimens tested for the planar mobility (see Table 1). For each joint, the maximal values were used for building the boundary lines.

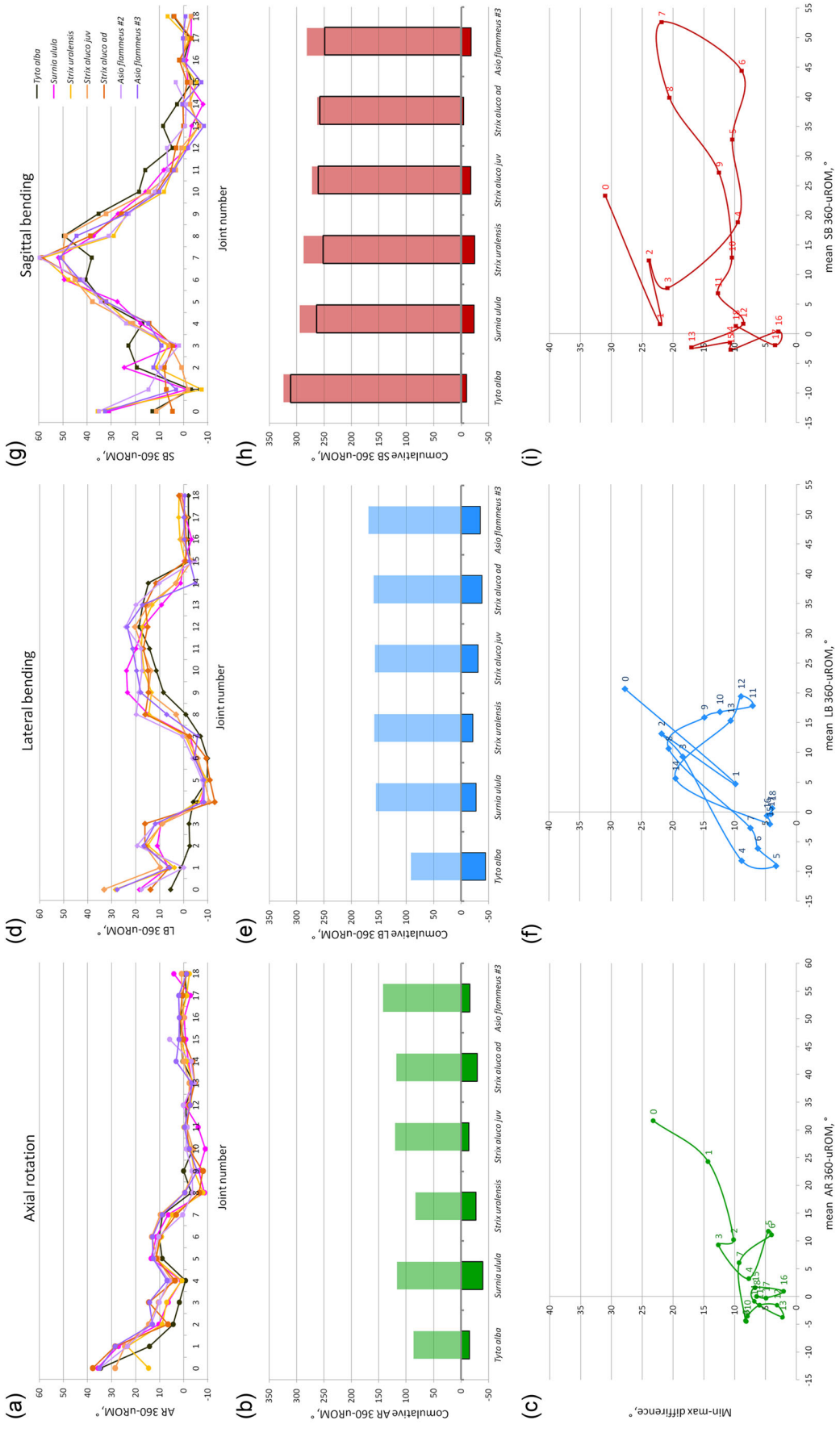

FIGURE 5 Angular ranges of motion used in 19 vertebral joints of owls during 360° head turn. (a, b, and c) Axial rotation (AR); (d, e, and f) lateral bending (LB); (g, h, and i) sagittal bending (SB). (a, d, and g) Joint-specific angles. (b, e, and h) Cumulative positive and negative angles throughout all 19 joints for axial rotation, lateral bending and sagittal bending (*Asio flammeus* #2 was excluded for nonreliable data on the last four joints); black frames in H highlight parts of SB bars corresponding to joints 1–18, that is, with exclusion of the occipital joint. (c, f, and i) Joint-specific min–max differences versus mean angles in the same joints.

head turn varied from 91° in *T. alba* to 169° in *A. flammeus* #3 (these sums are represented by the upper parts of bars in Figure 5e). The respective cumulative value for the joints bent to the opposite side varied from −21° in *S. uralensis* to −45° in *T. alba* (these are represented by the lower parts of bars in Figure 5e).

Among the studied specimens, the smallest maximum-to-minimum differences were found in joints 1, 4–7, 11 and 12 belonging to the neck, as well as in the intrathoracic joints 15–18 (Figure 5f). Of these joints, 4–7 had negative LB 360-uROMs, and in joints 15–18, the values varied near zero. The neck joints 11 and 12 are distinguished by the largest, among intervertebral joints, magnitudes of LB 360-uROM combined with small variation.

The largest interspecimen maximum-to-minimum differences in LB 360-uROMs were found in joints 2, 3 (cranial part of the neck), 8 (middle of the neck), and 14 (cervical-thoracic connection). The LB 360-uROM magnitudes in these joints are moderate.

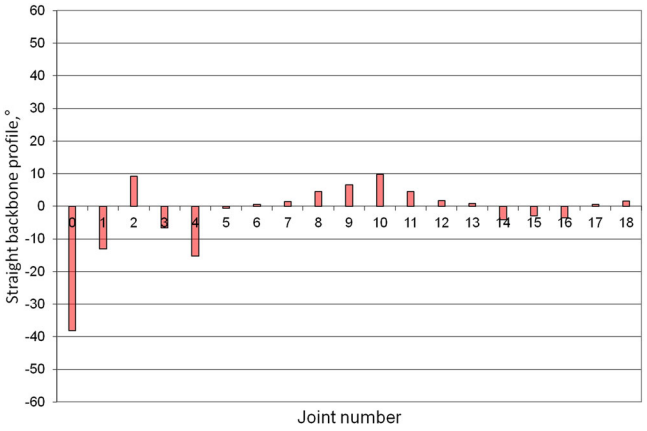

FIGURE 6 Angles formed in the sagittal plane by zygapophyses when the owl vertebral column is straightened. The bars represent joint-specific mean values averaged from the measurements on four specimens (see Table 1).

3.3 | Sagittal bending

3.3.1 | Straight position in the sagittal plane

SB fundamentally differs from AR and LB. The common feature of AR and LB is the inherent symmetry of motion to either side from the straight posture of the vertebral column associated with the plane of bilateral symmetry of the body. However, SB takes place in the plane of bilateral symmetry itself, known as the sagittal or median plane. Therefore, on the one hand, SB is characterized by a different range of motion to the dorsal and ventral sides of the straight posture. On the other hand, the average backbone position between the dorsal and ventral extremes is generally far from the straight posture. We did not consider the average posture and took the straight posture as the zero line for quantification of dorsal extension (positive) and ventral flexion (negative) in the sagittal plane.

Zygapophyses, which were the reference points in our calculations of intervertebral angles, have variable height along the backbone. Therefore, even in the perfectly straight backbone, the line drawn from zygapophysis to zygapophysis is not straight but forms a zigzag in the sagittal plane. The intervertebral angles of this zigzag line, averaged for four straightened specimens (Table 1), are shown in Figure 6. This profile characterizes the straight posture of the vertebral column of owls. The largest angle is found in joint number 1 (between the atlas and the epistropheus). It is negative as if the joint is bent ventrally, although the neck is actually straight. This is because the atlas-epistropheus zygapophysial points are located more dorsally than the respective points of the preceding occiput-atlas articulation and the subsequent articulation of the epistropheus with the third vertebra.

Hereinafter, all SB angles will be represented by net values obtained by subtracting the straight-backbone profile (Figure 6) from the raw measurements based on zygapophysial coordinates in the sagittal bent or 360°-turned specimens.

3.3.2 | Available dorsal bending in the sagittal plane: Dorsal part of SB planar-aROM

Two specimens of *A. flammeus* were studied with the neck bent dorsally (extended) in the sagittal plane; one of the specimens was dorsally bent and CT-scanned in this position two times. Taking, for each joint, the greatest value achieved in the three scans and summing them up for all 19 joints resulted in a cumulative deflection of 387° from the straight posture (Table S5). There was an uneven distribution of joint-specific angles of planar sagittal extension along the vertebral column (Figure 4c, upper line). The largest angle was found in joints 0, 5, and 8, while the smallest angles were close to 0° in joints 16–18 (caudal thorax). In the neck, the smallest angles of dorsal extension were found at the two ends—in the atlas-epistropheus joint and in joint number 13.

3.3.3 | Available ventral bending in the sagittal plane: Ventral part of SB planar-aROM

One specimen of *A. flammeus* (#1) was CT-scanned once with the neck bent ventrally (flexed) in the sagittal plane. We treat the ventral deflection from the straight posture as negative. The sum of planar flexion angles in all 19 vertebral joints of the studied specimen comprised −223°. The profile of distribution of ventral flexion along the vertebral column (Figure 4c, lower line) is generally shallower than the dorsal extension profile (Figure 4c, upper line), deviating more than the latter from the abscissa axis (which represents the straight posture) in joint 1 and three caudal joints of the neck. The largest negative angle was found in joint 13 (last intracervical), while the smallest angle was close to 0° in joint 16. In joint 7 (middle of the neck), ventral flexion was found to be impossible.

3.3.4 | Sagittal bending with full head turn: SB 360-uROM

In the specimens with the 360° head turn, the direction of SB in the neck is mainly dorsal (Figure 5g). In a few specimens, minor ventral bend was found in the first (atlas-epistropheus) joint. The largest dorsal bend was found in the middle of the neck. In the caudal part of the neck, the mean values of the dorsal bend steadily decreased from joint to joint. Beginning with joint 12 and through 18, SB angle varied around zero. The largest range of individual variation was found in the occipital joint due to our inability to keep the same pitching angle of the head in all specimens with the 360° head turn. Thus, the SB in the occipital joint is quite independent of the full head turn.

Discarding the occipital joint and considering the intervertebral joints 1–18, the sum of the angles of those joints which were bent dorsally during the 360° head turn varied from 249° in *A. flammeus* #3 to 311° in *T. alba* (Figure 5h, see black frames). The respective sum of the angles in the joints, which were bent ventrally varied from −5° in *S. aluco* ad. to −24° in *S. uralensis* (these are represented by the lower parts of bars in Figure 5h). The overall sagittal bend of joints 1–18 is given by the simple sum of the positive and negative angles (represented by the height difference of the upper and lower parts of bars in Figure 5h).

The smallest interspecimen maximum-to-minimum differences in SB 360-uROMs were found in joints 4, 6, 12 (neck), and 16–18 (thorax; Figure 5i). The largest differences were found in the neck joints 1–3, 7, 8. Of those, joints 7 and 8 were distinguished by very high mean SB 360-uROM values, while joints 1–3 had, on the contrary, relatively low mean SB 360-uROM values.

3.4 | Myology

A thorough dissection of *A. flammeus* and *S. ulula* revealed five portions in the m. intertransversarius (Figure 2). According to their topography, we named them as pars dorsalis, p. ventralis, p. profunda (also known as m. inclusius, not depicted in Figure 2), p. obliqua brevis, and p. obliqua longus. The first three run parallel to the longitudinal axis of the backbone. The oblique portions, which deviate from the longitudinal direction, appear to be a peculiarity of owls. Most unusual for birds in general is the p. obliqua longus, as it is the only part of the m. intertransversarius that is not a one-joint muscle but a two-joint muscle connecting even or odd vertebrae without attachment to an intermediate one. We found the two-joint p. obliqua longus in *S. ulula* but not in *A. flammeus*. It is noteworthy that even the one-joint portions of the mm. intertransversarii are distinguished in owls by shorter aponeuroses and longer muscle fibers than usual. Therefore, the muscle is not as pennate as in other birds and, due to relatively longer muscle fibers, allows for a relatively larger shortening range.

Three portions of the mm. intertransversarii of joints 4–10 were analyzed quantitatively in terms of shortening range: p. dorsalis, p. ventralis, and p. obliqua brevis. The p. obliqua longus, although it could belong to the set of specific morphofunctional adaptations of the owl neck, was discarded. Indeed, its absence in the studied specimen of *A. flammeus* casts doubt on its functional importance for owls. All seven 360°-turned specimens studied had a common pattern of muscle length distribution. All three measured portions of the mm. intertransversarii were longer on the side to which the head was turned than their counterparts in joints 4–7 and were shorter on this side in joints 8–10 (File S6). There were only two minor exceptions to this general rule. In the seventh joint of *S. uralensis*, the m. intertransversarius p. ventralis was slightly shorter on the side to which the head was turned than its counterpart, and in the eighth joint of *S. aluco* juv., the m. intertransversarius p. obliqua brevis was slightly longer on the side to which the head was turned.

The measured shortening percentages of mm. intertransversarii p. dorsalis, p. ventralis, and p. obliqua brevis of joints 4–10 obtained by comparing their lengths on the two sides of the 360°-turned specimens are presented in Figure 7. For each muscular portion, the interspecimen variation of the muscle shortening percentage values observed in each specific joint was 1.5–1.6-fold. The m. intertransversarius p. dorsalis showed the largest shortening percentages. In each specimen, the shortening percentages exceeded 30% in at least three joints. The largest joint-specific means of 41% were found in joints 9 and 10. The largest absolute maxima of more than 50% were found in the three posterior joints of *S. ulula*. The value of 57% in the 10th joint is the highest value in the whole sample of joints, specimens, and muscular portions. The m. intertransversarius p. ventralis showed intermediate shortening percentages. The joint-specific mean exceeded 30% in the 10th joint only, while the maximum never exceeded 50%. The m. intertransversarius p. obliqua brevis showed the smallest shortening percentages. The joint-specific mean reached 30% in neither joint. This limit was only exceeded in joints 5, 9, and 10 of *S. ulula*, with the values still below 40%.

In summary, the shortening percentages of the p. dorsalis, p. ventralis, and p. obliqua brevis were below 60%, 50%, and 40%, respectively. All three upper limits were most closely approached in the 10th joint (the caudal-most in the sample) of *S. ulula*. In fact, the limit of 50% was only exceeded by the p. dorsalis in the three joints (8–10) of *S. ulula*. The smallest shortening percentages of all three portions were found in the middle neck joint, number 7.

4 | DISCUSSION

4.1 | Axial rotation

In the specimens with the straight twisted neck, the cumulative AR of all 19 vertebral joints that were studied did not reach 190° from the nontwisted position to one side or the other. Thus, by itself, vertebral AR (including the occipital and the atlas-epistropheus joints) is not sufficient not only to produce the extreme 360° head turn but even to produce the 270° head turn from the resting position to one side or the other, frequently observed in live owls. Therefore, the 360° head turn is only possible with the head retraction into the shoulders

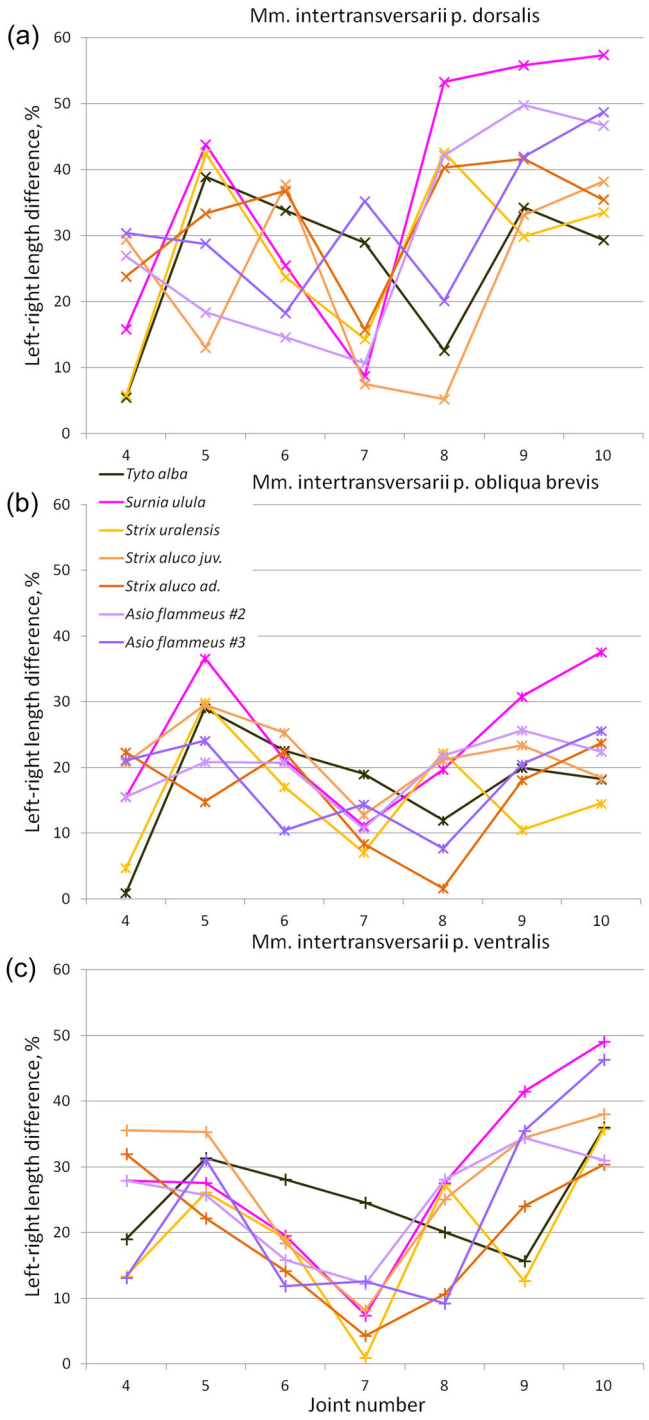

FIGURE 7 Shortening ranges (%) of pars dorsalis (a), p. ventralis (c), and p. obliqua brevis (b) of mm. intertransversarii in seven vertebral joints (4–10) used during 360° head turn in seven owl specimens.

by combining AR with LB and SB in the neck joints. The contribution of AR to this complex 3D motion needs to be considered.

The sum of joint-specific AR planar-aROMs throughout the backbone of the straight-twisted specimens could be compared to the simple sum of joint-specific AR 360-uROMs of the specimens with the full head turn. However, this comparison would underestimate the usage of available AR because, in the 360° head turn, some neck joints are considerably rotated in the opposite direction to the head turn. This was a highly unexpected finding, missed by previous researchers (Grytsyshina et al., 2016; Krings et al., 2017). Joints 8–13 were twisted to the "negative" side in all 360°-turned specimens. With simple summation, the AR 360-uROMs of these joints would be subtracted from the cumulative AR 360-uROM of the joints rotated in the positive direction (Figure 4), masking the overall usage of AR. Actually, the negative AR in joints 8–13 is as necessary for the peculiar 3D neck coiling during the full head turn as the positive AR in the other joints (an explanation will be provided after consideration of LB and SB). Therefore, for an adequate comparison of available and used AR, the sums of the absolute 360-uROM magnitudes in each joint should be considered. For the entire backbone (19 joints including the occipital one), this sum varied from 102° to 158° in different 360°-turned specimens, versus cumulative AR planar-aROM of 122°–182° (Table S5). Overall, the underuse of AR in the full head turn was about 20° when considering the entire backbone (joints 0–18) and 10° when considering the neck alone (joints 1–13).

4.1.1 | Are the limits of planar AR reached in the full head turn?

The overall underuse of available AR in the full head turn of 23° per 19 joints does not mean that it is equally distributed between the joints. Potentially, some joints could reach their AR planar-aROMs, and the others could even exceed the planar AR limits due to accompanying LB and SB, as suggested by some studies (Kambic et al., 2017; Krings et al., 2017). Actually, there was some variation across the seven 360°-turned specimens studied. Taking for each joint the maximal magnitude of AR 360-uROM found in the sample, it appears that, in most of the joints, the AR 360-uROMs, in one or the other specimen, coincide or closely approach the AR planar-aROMs (Figure 8a). It is worth noting that this is true for joint 4, which shows a drop in AR compared to the neighboring joints, both in the planar-aROM and in the 360-uROM. Considerable AR underuse is only found in joint 2 (6° or more). Neither one joint in any specimen shows a noticeably larger AR 360-uROM than the AR planar-aROM. The maximum overflow was 3°.

Therefore, it can be concluded that, during the full head turn of owls, LB and SB are used not for expansion of AR but for peculiar neck coiling. Overall, the AR is underused. The excess of available AR is responsible for the interspecimen variation in AR 360-uROM distribution along the backbone. Due to this excess, the joints in which AR 360-uROMs reached the AR planar-aROMs were different in different specimens. This means that an owl is free to vary the neck coiling a little during the full head turn. The most considerable underuse of AR was found in all specimens in the same joint—the caudal joint of the epistropheus (i.e., joint number 2). The underuse here was at least 6°. Probably, the excess AR planar-aROM observed in this joint is required for some other motions.

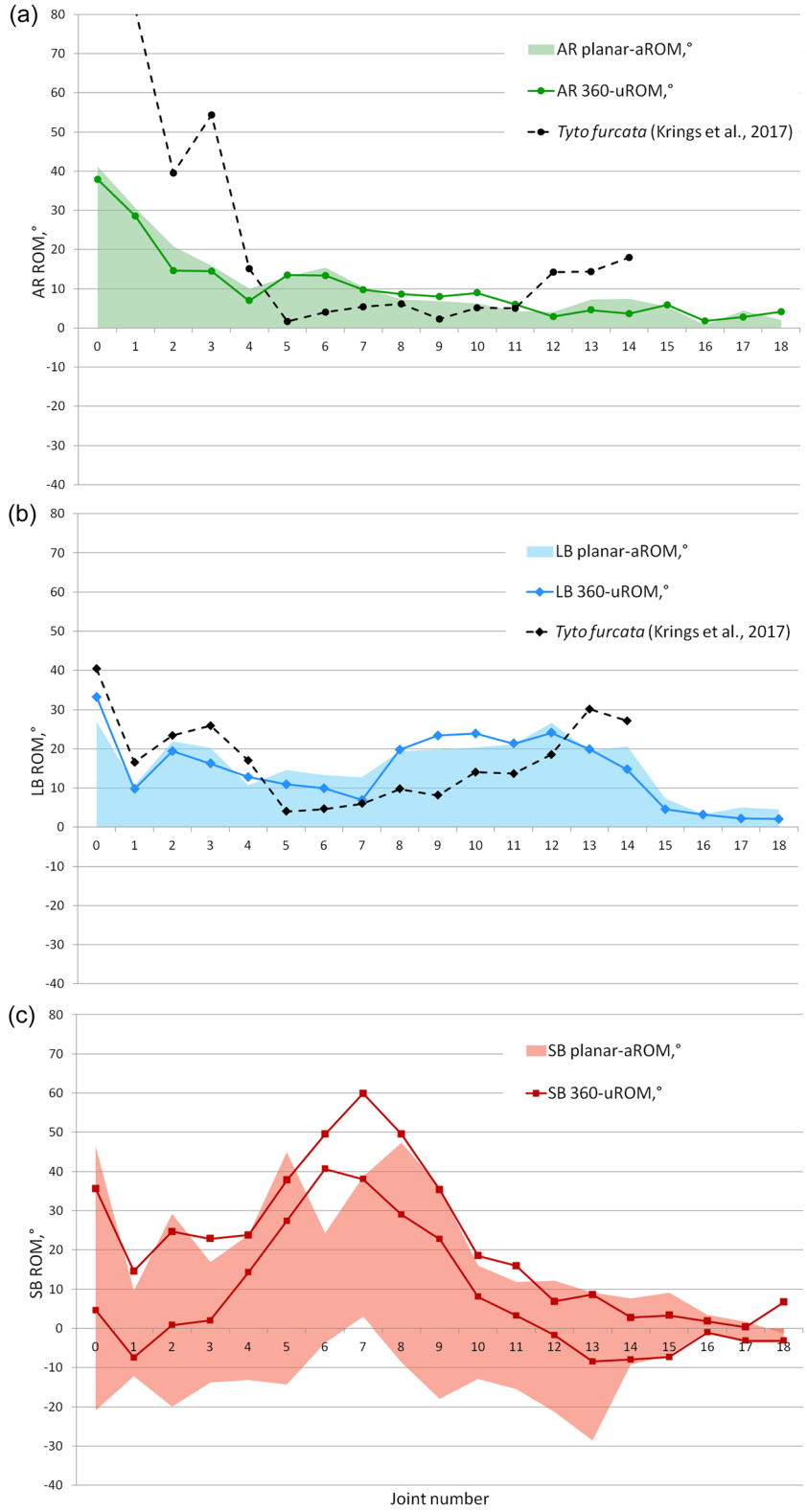

FIGURE 8 Comparison of joint-specific planar available ranges of motions (planar-aROMs) (filled areas) and 360 used ranges of motions (360-uROMs) (colored lines) of studied owl specimens. (a) Axial rotation, (b) lateral bending, (c) sagittal bending. The dashed lines are built based on in silico modeling of the vertebral aROMs in the barn owl (*Tyto furcata*) by Krings et al. (2017): in (a)—averaged α_y values, and in (b)—averaged β_r values from Supplementary tab. 1–4 of Krings et al. (2017.)

Comparison of our AR planar-aROM measurements on CT scans with the results of in silico modeling of owl's intervertebral AR mobility (Krings et al., 2017: averaged α_y values from Supplementary online material tab. 1–4; Figure 8a, dashed line) shows that the in silico modeling greatly overestimates the AR aROMs in the four cranial joints of the neck, especially in the occipital one. Smaller overestimation is found in the posterior part of the neck (joints 12–14). However, in joints 5, 6, and 9, the AR aROMs are considerably underestimated by in silico modeling. Most similar values are provided by both methods in joints 7, 8, 10, and 11. In our opinion, the overestimations and underestimations may result from the use of a different coordinate system for angle calculation and approximation of saddle-shaped joints with spheres by Krings et al. (2017). The extreme overestimation of AR aROM in the occipital joint most probably comes from the absence of bony limiters for AR at the occipital condyle.

4.2 | Lateral bending

The most striking feature of LB use in the full head turn was the presence, in all seven 360°-turned owl specimens, of a pronounced (up to −13° per joint) negative bend, that is, a bend to the opposite side than the head was turned. It was always found in joints 4–7, located just cranially to the middle of the neck. Joint number 8 is the joint where LB changes direction back from negative to positive, while AR changes from positive to negative. The joints with the largest LB magnitudes (ranging from +10° to +25° per joint) are joints 9–13, which form the posterior half of the neck.

In contrast to AR, LB does not exhibit a proportional relationship between the mean values of joint-specific 360-uROMs and their maximum-to-minimum ranges across studied specimens. The pattern is quite different (Figure 5f). Only in the occipital joint, the large mean is combined with a large range of variation. Among intervertebral joints, the largest maximum-to-minimum ranges were found in joints 2, 3, 8, and 14, characterized by medium LB 360-uROM magnitudes. Joints 11 and 12 had the largest LB 360-uROM magnitudes but a low maximum-to-minimum difference between specimens. This combination of a large mean and small variation manifests the crucial importance of joints 11 and 12 for accomplishing the full head turn in owls. Joints 4–7, with the negative LB direction, also showed low maximum-to-minimum differences, manifesting the importance of the negative bend. For comparison, the cranial neck joints 2 and 3, having positive LB 360-uROMs of approximately the same absolute magnitudes of ≈10° as joints 4 and 5, showed more than twice larger maximum-to-minimum differences. The low variation in the thoracic joints 15–18 is not surprising because they are poorly mobile, having LB 360-uROMs close to zero.

4.2.1 | Are the limits of planar LB reached in the full head turn?

The overall use of LB in the 360° head turn can be presented as the ratio of the sum of absolute magnitudes of joint-specific 360-uROMs (the absolutes are required because of the presence of negative LB in some joints of 360°-turned specimens) to the sum of maximal joint-specific LB planar-aROMs. For all 19 joints under study, the second sum taken for the denominator is 299°. In the seven 360-turned specimens, the sums of absolute 360-uROM magnitudes over the same 19 joints vary from ½ to ⅔ of that value. In other words, they did not use 32%–55% of available planar LB mobility in the full head turn. For the intracervical joints 1–13 alone, the cumulative LB planar-aROM angle is 231°, the cumulative of absolute 360-uROMs varies from ½ to ¾ of this value, and the remaining 27%–54% of planar LB mobility is unused in the full head turn.

Despite the rather large overall underuse of LB in each individual specimen with the 360° head turn, one or the other intervertebral joint in one or the other specimen reaches the LB angle corresponding to the planar mobility limit. Figure 8b presents joint-specific LB 360-uROM maxima found across the seven head-turned specimens compared to the respective LB planar-aROMs. A small enough overshooting of LB 360-uROM, by 2°–4° per joint, is found in joints 4, 9, and 10. Probably, the excess is false and comes from methodological limitations with planar bending. The LB planar-aROMs could be underestimated because we failed to reach the true bending limits in all joints together (see Section 2.7). In most of the 19 joints studied, the LB 360-uROMs do not exceed but closely approach the respective LB planar-aROMs, underusing it by 6° or less. In other words, the full head turn more or less completely exhausts the ability of these joints to bend laterally.

It should be remembered that Figure 8b presents joint-specific LB 360-uROM maxima found across the seven head-turned specimens. The maxima at different joints belong to different specimens. Respectively, depending on the specimen, the overall up to 50% LB underuse in the full head turn is dispersed over different joints. The interspecimen variability of distribution of the underused LB mobility from joint to joint implies that the degrees of freedom of the vertebral kinematic chain do not reach their limits all together in the 360° head turn. The arising freedom to redistribute the excess mobility confirms our hypothesis that the full head turn is not limited kinematically and, hence, is quite attainable by an owl in life. A live owl has the liberty not only to turn the head by 360° but also to do it with a variety of neck curvatures.

Comparison of our LB planar-aROM measurements on CT scans with the results of in silico modeling of owl's intervertebral LB mobility (Krings et al., 2017: averaged β_r values from Supplementary online material tab. 1–4; Figure 8b, dashed line) shows satisfactorily small differences in the cranial neck (joints 1–4) and at the neck–thorax transition (joints 13, 14). However, in the rest of the neck (joints 5–12), the in silico modeling produced about a twofold underestimation of LB aROMs, despite the fact that the method employed additional expansion of LB with the help of subsidiary AR. This dramatic underestimation may result from the use of a different coordinate system for angle calculation and approximation of saddle-shaped joints with spheres by Krings et al. (2017).

4.3 | Sagittal bending

The owls' backbone mobility in the sagittal plane is asymmetrical relative to the straight posture: available extension considerably exceeds available flexion. All 19 vertebral joints that were studied together allow for planar deflections of 387° to the dorsal side and (minus) 223° to the ventral side. The ratio of absolute magnitudes of these cumulative angles is 1.7. For the 13 intracervical joints, the respective ratio is as high as 1.8 in favor of extension (Table S5). It is worth noting that, generally, the backbone parts with a larger ability for extension show a larger ability for flexion, and the less extensible parts are also less flexible. Caudal neck joints are an exception.

Contrary to AR and LB, SB did not show a consistent alternation of deflections to one and the other side along the backbone in the 360°-turned specimens. There is not a single joint that was bent ventrally in all seven specimens. In some joints, namely 1 and 12–18, the SB angles fluctuated near zero from specimen to specimen. Joints 2–11 were bent dorsally in all specimens with the maximum angles in the middle neck joints 6–8. In the whole range of joints 2–12, the profile of extension angles roughly looks like a half-sine curve falling from the maximum in the middle to zero at the cranial and caudal ends. The SB maxima are by 20°–30° higher than the maxima of AR and LB. In joint 6, as well as joint 5, the large SB angles are combined with a small interspecimen variation thereof (Figure 5i), manifesting the crucial importance of these two joints in the 360°-turn performance.

The occipital joint (number 0) showed a relatively moderate mean SB angle of ≈25° directed dorsally, but an extremely high (>30°) maximum-to-minimum difference of SB angles across studied specimens (Figure 5i). This variance exceeds that in any other joint in SB, LB, and AR (Figure 5c,f,i). It implies that the SB mobility of the occipital joint is quite independent from the 360° head turn. Therefore, a live owl would not be restricted in head pitching and following vertical displacements of a prey object even in this extreme position.

4.3.1 | Are the limits of planar SB reached in the full head turn?

Discarding the occipital joint not involved in the 360° head turn, the overall angular limit of planar extension of owls' backbone is 340°. It is the sum of maximum deflections in the intervertebral joints 1–18 from the straight posture, measured in the specimens bent dorsally in the sagittal plane. In the same joint range, the sum of SB angles of the joints which were found to be bent to the dorsal side in the 360°-turned specimens varied from 249° to 311°. It is 8%–27% less than the available limit of 340°.

The joint-by-joint comparison of SB angles found in the planar-bent and the 360°-turned specimens shows the following (Figure 8c). In the dorsal extent, the SB planar-aROM profile more or less perfectly corresponds to the upper boundary of the SB 360-uROMs formed by the joint-specific maxima found in one or the other 360°-turned specimen. Contrary to that, the ventral extent of the SB planar-aROM profile is in most of the joints (except joints 1 and 14–18) far below the lower boundary of the SB 360-uROMs formed by the joint-specific minima found in one or the other 360°-turned specimen. This is an additional confirmation of the finding that the full head turn requires dorsal but not ventral bending of the backbone.

Most striking is the discrepancy between the SB planar-aROMs and the SB 360-uROMs in joints 6 and 7. These are the two cervical joints that show the largest 360-uROMs of all vertebral joints. Striking is that all the range of their 360-uROMs, including the lower boundary, is found well above the upper limits of planar extension available in these joints. The overshooting is especially large in joint 6, which we have pointed out in the previous subsection as one of the most crucial for the full head turn, based on the large angle of extension combined with small interspecimen variation of this angle. There may be two explanations for the overshooting of the 360-uROMs beyond the planar-aROMs. The first reason is technical and was noted in Section 2.7. We were restricted in the number of CT-scans and, therefore, could simply underestimate the planar-aROMs in some joints, being unable to bend all the joints together in the same direction. The second possible reason, suggested by some studies (Kambic et al., 2017; Krings et al., 2017), is the expansion of aROM in one direction of mobility, for example, SB, beyond its planar limit, due to motions in other directions, AR or LB. Although appealing, this explanation is hardly applicable in our case. Indeed, in the problematic joints 6 and 7, the AR and LB 360-uROMs are relatively low to have a considerable influence on SB aROM. In all studied specimens, the absolute magnitudes of AR and LB 360-uROMs were below 15° in joint 6 and below 10° in joint 7 (LB being negative in both joints). Much larger magnitudes of AR 360-uROMs in the cranial part of the neck and of LB 360-uROMs in the caudal part do not produce overshooting of SB 360-uROMs over planar aROMs. Therefore, we adhere to the technical explanation of the overshooting in joints 6 and 7 by underestimation of their SB planar-aROMs. Our data do not provide any confident example of considerable influence of one motion onto another, in respect of aROM, during the head-turning performance of owls.

4.4 | Distribution of AR, LB, and SB along the vertebral column in the full head turn

In the 360°-turned head position, different parts of the owl's backbone are characterized by larger or smaller intervertebral angles, which more or less follow aROM values (Figure 9). Rounding the minima and maxima, the 360° head turn employs AR from −10° (joints 8–10) to 35° (joint 0), LB from −10° (joints 4–6) to 35° (joint 0), and SB from −10° (joints 1, 13–15) to as much as 60° (joint 7). The large AR, LB, and SB angles do not coincide but alternate along the neck. The contribution of AR in the occipital joint (0) to the 360° head turn is not less than 15°–35°, the contribution of the occipital joint LB

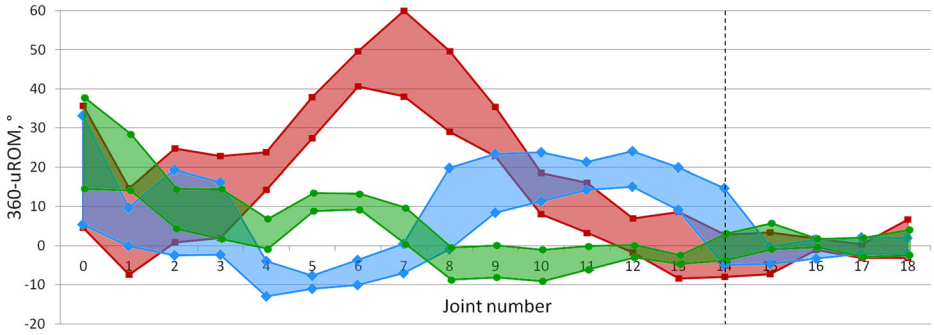

FIGURE 9 Maximum-to-minimum ranges of joint-specific 360 used ranges of motions (360-uROMs), that is, the axial rotation (green), lateral bending (blue), and sagittal bending (red) used during 360° head turn in 19 vertebral joints of five owl species (seven specimens studied). Dashed line indicates the neck–thorax boundary.

and SB is 5°–35°. The occipital joint has the maximal, and the atlas-epistropheus joint (1) submaximal AR angle in the whole backbone. Joints 2 and 3 are characterized by medium and almost equal angles in all three planes, with the smallest interspecimen variation being found in AR, and the largest one in SB. Beginning with joint 4, the angles in different planes become sharply unequal. Joints 4–7 located in the middle of the neck combine submaximal and maximal SB directed to the dorsal side, medium AR directed to the side of the head turn, and medium LB directed to the opposite side. The zone with submaximal SB continues caudally onto joints 8 and 9. The maximal LB is found in the caudal intracervical joints 9–13 and is directed there to the side of the head turn. So the joint number 9 is the point where the high SB changes for the high LB. The area of high positive LB (joints 9–13) almost coincides with the area of negative, although smaller in absolute magnitudes, AR (joints 8–13). Beginning with joint 14, 360-uROMs in all three directions fluctuate near 0°. So, not surprisingly, the contribution of the intrathoracic joints 15–18 to the 360° head turn is negligible.

The most peculiar feature of the intervertebral angles' distribution in the full head turn is that the direction of AR and LB is the same in the cranial-most joints 0–3 only. In the rest of the neck, where the SB angle rises to the maximum and falls to zero, the AR and LB angles have opposite directions and change in antiphase. In joints 4–7 AR angles are positive, and LB angles are negative, their absolute magnitudes being similar. Beginning with joint 8, the signs are reversed, although the absolute magnitudes become unequal with the predominance of LB. The exchange of signs between AR and LB coincides with the maximum SB angle. This point near joint 7 in the very middle of the neck is like the Gordian knot of the full head turn.

Our results confirm the conclusion of Krings et al. (2017), that the head turn of owls employs mainly AR ("yawing" of Krings et al.) in the cranial part of the neck, and LB ("rolling") in its caudal part. However, Krings et al. entirely excluded SB ("pitching") from analysis and, therefore, were unable to appreciate its crucial importance for the head-turning performance.

One of the most unexpected findings was the fact that in the 360° head turn a number of intervertebral joints were consistently (i.e., in all specimens studied) bent or twisted to the opposite side than the head was turned, as represented by negative LB and AR 360-uROMs, respectively. The negative angles are found in the loop formed by the neck above the shoulder toward which the head is turned, with negative LB in the cranial segment of this loop, and negative AR in the caudal one. We have checked on the virtual 3D model of *S. aluco*, what would occur if the negative angles were returned to zero in one or the other segment of the loop. Without the negative LB in the cranial segment, the head becomes inclined to the shoulder of the opposite side than the head is turned. Without the negative AR in the caudal segment of the loop, the head becomes inclined ventrally. Altogether, the negative angles allow keeping the cranial-most part of the neck (vertebrae I–IV) parallel to the thoracic backbone, negative LB being responsible for alignment in the frontal plane, negative AR for alignment in the sagittal plane. Due to this parallelism, the precise peering motions of the head, which are crucial for preattack prey detection (Barzilay et al., 2012, 2017; Ohayon et al., 2006), potentially, have to be minimally modified between the resting and the turned position. Underuse of AR, LB, and SB aROM in the neck of owls during the full head turn, which we have discovered, is probably a reserve required for retaining the ability for peering motions even in this extreme position.

4.5 | Comparison with other birds

Until now, data on the distribution of joint-specific aROMs along the backbone of birds have been scarce. The best-studied aROMs are those of SB; they were measured on fresh cadavers (ex vivo) in two palaeognathan genera (Cobley et al., 2013; Dzemski & Christian, 2007; van der Leeuw et al., 2001b), a number of anseriforms (Landolt et al., 1989; van der Leeuw, 1991; van der Leeuw et al., 2001a, 2001b; Zarnik, 1926; Zweers et al., 1994), and the domestic chicken (*Gallus gallus*; Landolt et al., 1989; van der Leeuw et al., 2001a, 2001b; Zweers et al., 1987, 1994). In contrast, ex vivo measurements of AR aROMs are almost unavailable, except for a few joints (Kambic et al., 2017; Zarnik, 1926). The distribution of both SB and LB along the whole neck was only studied in the domestic goose (Zarnik, 1926) and the common ostrich (*Struthio camelus*; Cobley

et al., 2013; Dzemski & Christian, 2007). With the scarcity of data, a useful first approximation to understanding owls' position in the general avian diversity is to compare our estimates of LB and SB planar-aROMs in owls with the respective values, also measured as planar deviations of the neck from the straight posture, reported for the domestic goose (Zarnik, 1926) and the ostrich (Dzemski & Christian, 2007) for all intracervical and the cervical-thoracic joint. The comparison is presented in Figure 10. The number of cervical vertebrae is 14 in owls, 16 in the goose, and 18 in the ostrich. Therefore, for a correct comparison of their neck mobility, we adjusted the horizontal scales of the graphs so that the occipital and cervical-thoracic joints match across the three birds. Zarnik (1926) did not divide SB planar-aROM into the dorsal part (extension) and the ventral part (flexion). Therefore, for a correct comparison with the goose, we had to sum up, for each joint, the absolute magnitudes of extension and flexion found in owls (our data) and ostriches (data from Dzemski & Christian, 2007: Figure 7).

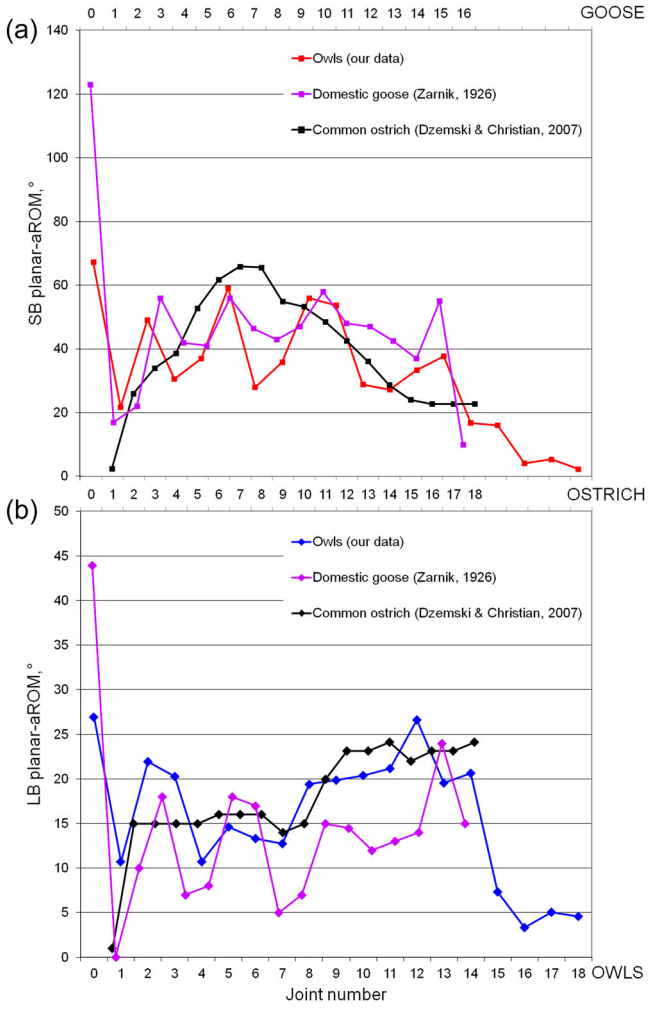

FIGURE 10 Planar available ranges of motions (planar-aROMs) of owls (our data), goose (after Zarnik, 1926), and ostrich (recalculated from Dzemski & Christian, 2007: Figure 7). The horizontal scales of the three curves are adjusted by the occipital joint (number 0) and cervical-thoracic joint (number 14 in owls, 16 in goose, and 18 in ostrich). (a) Sagittal bending (extension + flexion); (b) lateral bending (to one side from the straight posture).

All three birds exhibit quite similar SB planar-aROM magnitudes. The mean values for the intracervical joints 1–13 in owls, joints 1–15 in the goose, and joints 1–17 in the ostrich are 38°, 44°, and 40°, respectively, which are very close to each other. The cumulative intracervical SB planar-aROMs differ according to the number of neck joints: 498° in owls, 658° in the goose, and 680° in the ostrich. The profile of distribution of the joint-specific SB planar-aROMs along the neck is generally similar in the three birds (Figure 10a). The ostrich profile is smoother. The profiles of owls and the goose are more jagged, with a surprisingly close coincidence of the local minima and maxima between the two. Overall, it can be concluded that the SB aROM is not increased in owls. What is required for the 360° head turn in owls appears to be as useful for other activities in geese, ostriches, and probably many other birds not yet studied in respect of neck mobility. One of the crucial activities may be grooming, especially cleaning the feathers on the back.

The profile of LB planar-aROM distribution along the neck is also quite similar in the three birds (Figure 10b). Again, the profile of the ostrich is smoother, and those of owls and the goose are more jagged, with a close coincidence of the local minima and maxima between the two. However, there is an important difference in the LB planar-aROM magnitudes (not found in the case of SB). The difference is found in the caudal half of the neck between the goose, on the one hand, and the owls with the ostrich, on the other hand. In the middle, the LB planar-aROM leaps to higher values in the owls and the ostrich but does not in the goose. The profiles remain parallel, but the angular magnitudes of the goose are about two-fold smaller in this part of the graph than those of the other two. The mean LB planar-aROMs for joints 1–13 in owls, joints 1–15 in the goose, and joints 1–17 in the ostrich are 18°, 12°, and 17°, respectively. The cumulative intracervical LB planar-aROMs are 231° in owls, 183° in the goose, and 297° in the ostrich. It should be remembered that these values represent the bend from the straight position to one side. The full left-to-right range is represented by double angles; thus, the mean left-to-right LB planar-aROMs are 36° in owls, 24° in the goose, and 35° in the ostrich. These values can be compared to the full flexion-to-extension SB planar-aROM mean values presented in the previous paragraph: 38° in owls, 44° in the goose, and 40° in the ostrich. Thus, available SB exceeds LB in all those birds, but in owls, the difference is negligible. The most pronounced difference is found in the goose because of the aforementioned absence of rise of LB planar-aROMs in the caudal half of the goose neck. Our preceding analysis has shown the crucial importance of high LB planar-aROMs in the caudal part of the neck of owls for the 360° head turn. However, why it is as much developed in the ostrich is a puzzle for future research.

Kolmogorov–Smirnov (K–S) two-sample test allows to compare the SB and LB planar-aROM profiles of owls (joints 1–14), goose (joints 1–16), and ostrich (joints 1–18) quantitatively. The online calculator ("Quest Graph™ K–S Test Calculator." *AAT Bioquest, Inc.*, January 26, 2023, https://www.aatbio.com/tools/kolmogorov-smirnov-k-s-test-calculator) provides the following p-values for

pairwise comparisons. For SB: owls versus ostrich $p = .8625$ (very high similarity), ostrich versus goose $p = .3797$, goose versus owls $p = .08$. For LB: owls versus ostrich $p = .4055$, ostrich versus goose $p = .0228$, goose versus owls $p = .0131$. Only the last two values are below .05, which means that the neck LB of the goose is significantly different from that of the ostrich, and even more significantly different from that of the owls. The ostrich appears to be as similar to owls in LB as it is similar to goose in SB. In both SB and LB, the greatest similarity is found between the owls and the ostrich, and the smallest similarity is between the owls and the goose. The ostrich–goose pair is intermediate in both SB and LB.

The AR planar-aROMs are unavailable for the ostrich. For the goose, Zarnik (1926) only measured twisting in the first two vertebral joints: 33° in the occipital joint and 17° in the atlas-epistropheus joints. In the owls, our measurements of AR planar-aROMs in the same joints reach 41° and 31°, respectively, which is about 10° more in each one than in the goose. The addition of these ≈20° is not a small contribution to the 360° head turn. However, AR in subsequent joints is questionable. From a theoretical standpoint, the heterocoelous (saddle-shaped) intervertebral joints of birds are biaxial, meaning their mobility is restricted to SB and LB, while AR is reduced to zero (Abourachid et al., 2021; Furet et al., 2021). On the other hand, the almost entire lack of data on AR in the avian neck and claims of its absence (e.g., zero values of AR in joints 2–16 of the goose presented by Zarnik, 1926) may not come from its theoretically expected absence but from the fact that it is extremely difficult to make measurements of intervertebral twisting angles. The recent ex vivo measurements of angular limits of motion in selected neck joints of a turkey (Kambic et al., 2017) have shown theoretically unexpected high values of AR. These were joints 3, 4, 5, 6, 8, and 9 (number 7 was discarded for technical reasons). The sum of AR aROMs in those six joints, when measuring from the straight position to one side extreme, was found to comprise 71° during combined motion in three planes (recalculated from Kambic et al., 2017: figure 10) and 34° during planar motion (recalculated from Kambic et al., 2017: figure 6b). In our terminology, the latter value is the cumulative AR planar-aROM. In owls which we have studied, the respective value for the same six joints is, on average, 68°, which is twice more than in the planar neck twisting of the turkey and almost equal to the AR aROM of the latter in combined motion, when twisting is facilitated by simultaneous LB and SB. Our data do not show enlarged AR amplitudes in the neck of owls during the 360° head turn, when AR is combined with LB and SB, compared to planar AR motion. However, we can contend that AR planar aROMs of owls considerably exceed those of the goose in joints 0 and 1 and those of the turkey in joints 3, 4, 5, 6, 8, and 9. This allows us to propose that an extended ability for planar twisting of the neck is one of the major keys to the ability of owls to turn the head more than other birds.

4.6 | Mm. intertransversarii as natural goniometers of neck joints

Krings et al. (2017) expressed doubt about whether the neck muscles are able to turn the owl's head in life as much as the dead specimen allows. They did not specify the reasons for this supposed muscular inability. Most probably, it was meant that the length of muscle fibers is insufficient for such a range of motion. This is an issue that needs to be addressed.

Considering the limits of mobility in individual joints, one-joint muscles are the most informative. They can be treated as natural goniometers, in fact. One-joint muscles represent a primitive (myomeric) condition of axial musculature in vertebrates. The avian neck musculature is basically composed of three parts: dorsal, lateral, and ventral (e.g., Boas, 1929; Böhmer et al., 2020; Kuroda, 1962; Landolt & Zweers, 1985). The dorsal and the ventral muscles operate SB, and the lateral ones operate LB. One-joint muscles are lost in the ventral musculature of birds and are poorly preserved in the dorsal musculature, being represented there by tiny mm. interspinales in the cranial part of the neck (joints 2–4), and mm. intercristales in the middle and caudal part (beginning with joint 5). Boas (1929) reports complete loss of the mm. intercristales in *Bubo bubo*. The mm. interspinales span the usual number of joints (2–4) in *Bubo bubo* (Boas, 1929) but only joints 2 and 3 in *S. aluco* (Boas, 1929) and joint number 2 alone in *T. furcata* (Boumans et al., 2015). In contrast, one-joint muscles are dominant in the lateral musculature, being represented by mm. intertransversarii. They cover the lateral aspect of the avian neck with a thick continuous, although segmented layer. Each segmental m. intertransversarius has a complicated 3D architecture with multiple pennation (Baumel et al., 1993; Landolt & Zweers, 1985; Zusi & Storer, 1969). The muscular belly is penetrated by a large number of aponeuroses arising from the vertebral transverse processes and the cervical ribs, as well as from the articular processes (zygapophyses). The mm. intertransversarii of owls have not been specially studied yet (Boumans et al., 2015).

The m. intertransversarius pars obliqua is the most oblique, and thus most appropriate for AR operation, of all neck muscles known in birds. The pars obliqua longus found in *S. ulula* is not as oblique as the pars obliqua brevis, making it less efficient for AR. The pars obliqua longus is a rather unusual two-joint element in the lateral neck musculature of birds and was previously reported for some neck segments of the heron *Ardea* (Boas, 1929) and duck (Landolt & Zweers, 1985). A more profound feature of owls is that their mm. intertransversarii show a less complex pennation than is known in other birds (Landolt & Zweers, 1985; Zusi & Storer, 1969). The bulk of muscle fibers of an owl's m. intertransversarius are long enough to cover the full distance from the point of origin on one vertebra to the point of insertion on the next one. Increased muscle fiber length is an evident adaptation to increased angular mobility in the respective joint. The presence of especially long-fibered m. intertransversarius pars obliqua longus in *S. ulula* is consistent with the fact reported above, that of all seven 360°-turned specimens, it was *S. ulula* that showed the largest shortening percentages in all three measured portions of the mm. intertransversarii. The maximal shortening percentages were found in joints 9 and 10 of *S. ulula*. These two joints were distinguished in *S. ulula* by larger LB 360-uROMs than in other owls studied (Figure 5d). Thus, the rare two-joint portions of the mm. intertransversarii appear to be perfectly consistent with the

increased LB 360-uROMs, whether it is a species-specific feature of *S. ulula* or an individual variation of the specimen that we had the opportunity to study.

The oblique portions of mm. intertransversarii found in owls are useful not only with respect to AR actuation but also with respect to increasing the efficiency of LB actuation. Indeed, in 360°-turned specimens, the pars obliqua brevis mainly showed shortening percentages below 30% (except for three joints of *S. ulula* with shortening percentages between 30% and 40%). At the same time, the pars recta ventralis mainly showed shortening percentages of up to 40% (two joints of *S. ulula* and one joint of *A. flammeus* #3 had percentages between 40% and 50%). The pars recta dorsalis mainly showed shortening percentages of up to 50% (three joints of *S. ulula* had percentages between 50% and 60%). The smaller degree of shortening in oblique compared to longitudinal muscle fibers during LB was profoundly modeled for myomeres of swimming fish (Alexander, 1969) and urodelan amphibians (Azizi & Brainerd, 2007; Brainerd & Azizi, 2005). The cosine of muscle fiber angle to the longitudinal body axis is converted into a lower-than-1 ratio of (longitudinal strain/fiber strain), which was termed the architectural gear ratio (Azizi & Brainerd, 2007; Brainerd & Azizi, 2005). The more muscular fibers decline from the horizontal (more specifically, from the frontal plane of the body), the less they have to shorten for a given amount of longitudinal strain. This is what we observed in owl specimens with smaller shortening ranges of the oblique portions of the mm. transversarii compared to the longitudinal portions of the same muscles in the same joints. The smaller the fiber shortening percentage required from a muscle, the better it can be adjusted to the most forceful part of the sarcomere's force-length curve by optimizing the number of sarcomeres in a fiber (e.g., Alexander, 1989). The shortening range below 30% and rarely up to 40%, found in the oblique portions of the 360°-turned specimens, perfectly fits the known ranges of efficient contraction of skeletal muscles. This means that the m. intertransversarii pp. obliqua breves are perfectly adapted to ensure the full 360° turn of the head.

It should be remembered that the skeletal movement, on which the length of a muscle depends is the very movement that this muscle controls. It is quite evident from the topography (Figure 2) that the lengths of the mm. intertransversarii p. dorsalis and p. ventralis are primarily related to LB, while the lengths of the oblique portions depend on both LB and AR. Shortening of the left p. dorsalis and p. ventralis is associated with LB of the respective neck joint to the left side, and shortening of their right counterparts is associated with LB to the right side. Shortening of the oblique portions is associated with LB to the same side where they are located and AR to the opposite side. This LB-AR opposition in the action of the oblique portions is concordant with the LB-AR opposition of joint angles during the 360° head turn all over the owl's neck from joint 4 to joint 13 inclusive (Figure 9). It was reported above that in joints 4–7, the positive AR is combined with the negative LB, and the signs are reversed in joints 8–13. This means that not only the longitudinal pp. dorsales and pp. ventrales but also the oblique portions of the mm. intertransversarii can be expected to be shorter on the side of the head turn in joints 8–10 and on the opposite side in joints 4–7. This is exactly what was shown by our measurements of muscle lengths (File S6). Thus, the functions derived from topography are proved.

4.7 | Is the shortening range of the mm. intertransversarii required for the full head turn realistic?

The shortening percentages found in the longitudinal p. dorsalis and p. ventralis were larger and may seem problematic. Especially large was the shortening percentage required from the p. dorsalis. Our data can be compared with the shortening ranges of various skeletal muscles of a number of vertebrates, as reviewed by Burkholder and Lieber (2001). In their tab. 2, the longest and shortest sarcomere lengths of a given muscle of a given animal are presented in µm. The difference between the two values divided by the larger one gives the shortening percentage directly comparable to our data. Percentages from 40% to 50% were found in human m. vastus lateralis, m. vastus medialis, and m. temporalis, rat's m. gastrocnemius, cat's m. biceps femoris, and rabbit's m. gastrocnemius lateralis. A 50% shortening was found in the cat's m. soleus, and 51% in the rabbit's m. rectus femoris. The last value comes from one of the most methodologically reliable sources (Dimery, 1985). The cases with higher shortening percentages were treated by Burkholder and Lieber as outliers. In the full head turn of the owls under study, the limit of 50% was only exceeded by the m. intertransversarius p. dorsalis of joints 8 (53%), 9 (56%), and 10 (57%) in *S. ulula*.

It can be concluded that the shortening percentages required for the 360° head turn from all three studied portions of the mm. intertransversarii are not outstanding compared to skeletal muscles of other vertebrates (three outliers per 147 measurements). It is worth noting that only three avian muscles were included in the review by Burkholder and Lieber (2001). Of those three, the m. pectoralis and m. supracoracoideus had shortening percentages as low as 11%–23%, while the "patagialis muscle" (most probably it is the m. deltoideus propatagialis) showed a shortening percentage of 31%. All these muscles belong to the flight apparatus and, thus, are, to a greater or smaller extent, responsible for body weight support. However, the neck muscles of owls, when coiling the neck to turn the head, have to support the weight of the head alone. Therefore, the flight muscles should most probably operate in the best part, that is, the plateau, of the sarcomeres' force-length curve, while the neck muscles may be allowed to employ a wider part of this curve, including its suboptimal limbs at the sides of the plateau. Previously, the descending limb of the force-length curve, where sarcomere lengths are larger than the optimum, was thought to be poorly used. This condition was thought to be mechanically unstable because in this limb, the force is reduced with length, and, hence, individual sarcomeres, which are occasionally longer, would be stretched more and more by their shorter neighbors (Morgan, 1990). However, the descending limb is now found to be extensively used in reality (Burkholder & Lieber, 2001: Figure 2), and its mechanical stability is

theoretically approved through the force-velocity relationship (Azizi & Dunlevie, 2014). A longer sarcomere, when being forcibly stretched, becomes stronger than its shorter neighbors, and their lengths automatically equalize.

To summarize, the mm. intertransversarii of owls appear to be specially adapted to actuate the neck during extreme head turns while following the prey with the gaze. They have a reduced pennate structure in favor of long muscular fibers to allow for increased angular motions in the intervertebral joints. They acquired the oblique portion which is not only the best muscle for neck twisting hitherto known among birds but is also more efficient in large-range LB than the usual longitudinal portions are.

5 | CONCLUSIONS

This study of the mechanism of the extreme head turn of owls has broad implications for research on backbone function. It provides a new CT-scan-based method for measuring intervertebral joint angles using an anatomically meaningful JCS, and will hopefully stimulate future studies of complex 3D motions of the vertebral column in a variety of birds and other vertebrates.

Our first hypothesis was that in different owl species, the 360° head turn is achieved ex vivo with a similar, quite regular, and specific posture of the neck. It was proved to be true. Indeed, the general pattern of neck coiling in the 360°-turned head position is shared by all owls studied, although there remains considerable variability in specific values of joint angles. The second hypothesis of the existence of extraordinary vertebral mobility in owls, compared to other birds, is confirmed but only partially. The available range of sagittal bending (SB planar aROM) in the neck joints of owls is close to that of the ostrich and goose. The available range of lateral bending (LB planar aROM) in the neck joints of owls is close to that of the ostrich, but the goose differs from both the owls and the ostrich by about twice restricted lateral mobility in the caudal part of the neck. Thus, the goose appears to be a more deviant case than owls. As for axial rotation, the data on other birds are scarce. However, the available data on joints 0 and 1 of the goose and on six middle-neck joints of the turkey mildly suggest that owls do exceed other birds in the available range of vertebral twisting (AR planar-aROM), thus breaking the theoretical presumption that the saddle-shaped intervertebral joints of birds are biaxial in principle. Regarding combined angulation of a joint in three planes, it appears, in general, not to expand the range of motion in any of them compared to planar motions in owls. Thus, the three degrees of freedom appear to be quite independent in respect of the maximum available amplitude. The only probable, although equivocal, exception is the hyperextension in the middle of the neck (joints 6 and 7) found in the 360°-turned specimens but not in the specimens bent in the sagittal plane. In the other joints and in all three planes of motion, the available planar ranges of motion were more or less completely used in the full head turn but not considerably surpassed.

On the whole, during the full head turn, the maximal joint angles in three planes alternate along the neck. In joints 0 and 1, axial rotation tends to exceed lateral and sagittal bending, which are mutually equal. In joints 2 and 3, all three angle components are roughly equal to each other. From joint 4 through joint 13, the maxima alternate: the maximal axial rotation (to the side of head turn) is followed by the maximal sagittal bending (in ventral direction) and then by the maximal lateral bending (to the side of head turn). Of those three, the maximum of sagittal bending is the highest, being roughly 2.5 times higher than the lateral bending maximum in the posterior part of the neck and 5 times higher than the axial rotation maximum in the anterior part, and even two times higher than the axial rotation in the occipital joint. Quite expectedly, the thoracic region shows small joint angles in all three planes and, thus, has no significant contribution to the head turn.

Overall, the available mobility is somewhat underused in every direction during the 360° head turn. Therefore, an owl is free to distribute this extra mobility along the neck. This freedom was expressed in our sample as the interspecimen variation of the joint angles. Thus, in different 360°-turned specimens, the available angular limits were reached in different joints. Not a single specimen reached the maximal available angles in all the vertebral joints together in any direction.

An unexpected but necessary feature of the 360° head turn is the lateral bending (joints 4–7) and axial rotation (joints 8–13) to the opposite side than the head is turned. Contrary to that, the bending in the sagittal plane involved in the full head turn is unidirectional. It is either directed to the dorsal side or varies from specimen to specimen near zero. Neither one joint showed bending to the ventral side in all the specimens studied.

The negative LB and AR angulation in certain neck joints during the full head turn keeps the cranial part of the neck parallel to the thoracic spine. We hypothesize that this parallelism may ensure the reduction of possible interference of the head turning, required to visually seek and follow prey, with the head peering, required to detect it. Further, we hypothesize that the overall underuse of aROM in the neck, which we have discovered in the full-head-turned specimens of owls, is that kinematic reserve, which allows performing independent peering motions simultaneously with head turning.

The peculiar 3D coiling of the neck, ensuring the full head turn, requires joint-specific muscular control with one-joint muscles mainly located on the lateral sides of the neck—the mm. intertransversarii. The shortening ranges required for the 360° head turn of the portions of the mm. intertransversarii in the middle (most coiled) region of the neck were found to fit the normal shortening ranges known for the skeletal muscles of vertebrates. Thus, our third hypothesis was proved to be true. The oblique portions of the mm. intertransversarii, well-developed in owls but not yet reported for other birds, show the smallest shortening range during the full head turn and, hence, are most efficient for the performance of this motion. Therefore, the oblique portions present a special adaptation to the extreme head turn. This is what we have hypothesized: the special rearrangement of neck muscles on the macro-morphological

level allows the production of the 360° head turn while keeping muscular contraction in the suboptimal, if not perfectly optimal, range.

The discovered morpho-functional features of joints and muscles of the owl's neck provide strong evidence in favor of the hypothesis that these birds are actually capable of making the 360° head turn in life, although such turns have not yet been reported in nature or captivity. This is a task for future experimental investigation.

AUTHOR CONTRIBUTIONS

Aleksandra A. Panyutina performed CT-scan processing, made illustrations, performed calculations, and wrote text. Alexander N. Kuznetsov made mathematical model, performed calculations, and wrote text.

ACKNOWLEDGMENTS

Ekaterina E. Grytsyshina initiated this research being a student of the authors, and they could not stop turning heads in more and more owls. Yaroslav A. Red'kin, Arkady B. Savinetsky, and Alexander S. Savin provided some of the specimens for these exercises. Nadezhda V. Kryukova helped with CT scan processing. Alexander B. Savinetsky gave valuable advice on the application of the Kolmogorov–Smirnov test.

DATA AVAILABILITY STATEMENT

The data supporting the findings of this study are available in the supplementary material to this article. The original CT scans are uploaded to the morphosource.org repository https://www.morphosource.org/projects/000549076/ and available on request.

ORCID

Aleksandra A. Panyutina http://orcid.org/0000-0002-8379-8526
Alexander N. Kuznetsov https://orcid.org/0000-0002-9928-6955

PEER REVIEW

The peer review history for this article is available at https://www.webofscience.com/api/gateway/wos/peer-review/10.1002/jmor.21669.

REFERENCES

Abourachid, A., Gagnier, B., Furet, M., Cornette, R., Delapre, A., Hackert, R., & Wenger, P. (2021). Modeling intervertebral articulation: The rotule à doigt mechanical joint (RAD) in birds and mammals. *Journal of Anatomy*, *239*(6), 1287–1299. https://doi.org/10.1111/joa.13517

Alexander, R. M. (1969). The orientation of muscle fibres in the myomeres of fishes. *Journal of the Marine Biological Association of the United Kingdom*, *49*(2), 263–290. https://doi.org/10.1017/S0025315400035906

Alexander, R. M. (1989). Muscles for the job. *New Scientist*, *1660*, 50–53.

Azizi, E., & Brainerd, E. L. (2007). Architectural gear ratio and muscle fiber strain homogeneity in segmented musculature. *Journal of Experimental Zoology Part A: Ecological Genetics and Physiology*, *307*(3), 145–155. https://doi.org/10.1002/jez.a.358

Azizi, E., & Dunlevie, M. D. (2014). Boundaries of skeletal muscle instability at long sarcomere lengths. *Integrative and Comparative Biology*, *54*, E8.

Barzilay, O., Gutfreund, Y., & Wolf, A. (2012). Biokinematic study of barn owl head movements for the development of a bio-inspired active vision robotic system. In J. Lenarcic & M. Husty (Eds.), *Latest advances in robot kinematics* (pp. 139–146). Springer. https://doi.org/10.1007/978-94-007-4620-6_18

Barzilay, O., Zelnik-Manor, L., Gutfreund, Y., Wagner, H., & Wolf, A. (2017). From biokinematics to a robotic active vision system. *Bioinspiration & Biomimetics*, *12*(5), 056004. https://doi.org/10.1088/1748-3190/aa7728

Baumel, J. J. (1993). Handbook of avian anatomy: *Nomina anatomica avium*, 2nd edition. (p. 23). Publications of the Nuttall Ornithological Club.

Belyaev, R. I., Kuznetsov, A. N., & Prilepskaya, N. E. (2021a). A mechanistic approach for the calculation of intervertebral mobility in mammals based on vertebrae osteometry. *Journal of Anatomy*, *238*(1), 113–130. https://doi.org/10.1111/joa.13300

Belyaev, R. I., Kuznetsov, A. N., & Prilepskaya, N. E. (2021b). How the even-toed ungulate vertebral column works: Comparison of intervertebral mobility in 33 genera. *Journal of Anatomy*, *239*(6), 1370–1399. https://doi.org/10.1111/joa.13521

Belyaev, R. I., Kuznetsov, A. N., & Prilepskaya, N. E. (2022). From dorsomobility to dorsostability: A study of lumbosacral joint range of motion in artiodactyls. *Journal of Anatomy*, *241*(2), 420–436. https://doi.org/10.1111/joa.13688

Boas, J. E. V. (1929). Biologisch-anatomische studien über den hals der vögel. *Kongelige Danske Videnskabernes Selskabs Skrifter*, *9*(1), 101–222.

Böhmer, C., Prevoteau, J., Duriez, O., & Abourachid, A. (2020). Gulper, ripper and scrapper: Anatomy of the neck in three species of vultures. *Journal of Anatomy*, *236*(4), 701–723. https://doi.org/10.1111/joa.13129

Boumans, M. L. L. M., Krings, M., & Wagner, H. (2015). Muscular arrangement and muscle attachment sites in the cervical region of the American barn owl (*Tyto furcata pratincola*). *PLoS ONE*, *10*(7), e0134272. https://doi.org/10.1371/journal.pone.0134272

Burkholder, T. J., & Lieber, R. L. (2001). Sarcomere length operating range of vertebrate muscles during movement. *Journal of Experimental Biology*, *204*(9), 1529–1536. https://doi.org/10.1242/jeb.204.9.1529

Brainerd, E. L., & Azizi, E. (2005). Muscle fiber angle, segment bulging and architectural gear ratio in segmented musculature. *Journal of Experimental Biology*, *208*(17), 3249–3261. https://doi.org/10.1242/jeb.01770

Cobley, M. J., Rayfield, E. J., & Barrett, P. M. (2013). Inter-vertebral flexibility of the ostrich neck: Implications for estimating sauropod neck flexibility. *PLoS ONE*, *8*(8), e72187. https://doi.org/10.1371/journal.pone.0072187

Dimery, N. J. (1985). Muscle and sarcomere lengths in the hind limb of the rabbit (*Oryctolagus cuniculus*) during a galloping stride. *Journal of Zoology*, *205*(3), 373–383. https://doi.org/10.1111/j.1469-7998.1985.tb05623.x

Dzemski, G., & Christian, A. (2007). Flexibility along the neck of the ostrich (*Struthio camelus*) and consequences for the reconstruction of dinosaurs with extreme neck length. *Journal of Morphology*, *268*(8), 701–714. https://doi.org/10.1002/jmor.10542

Furet, M., Abourachid, A., Böhmer, C., Chummun, V., Chevallereau, C., Cornette, R., De La Bernardie, X., & Wenger, P. (2021). Estimating motion between avian vertebrae by contact modeling of joint surfaces. *Computer Methods in Biomechanics and Biomedical Engineering*, *25*(2), 123–131. https://doi.org/10.1080/10255842.2021.1934676

Fux, M., & Eilam, D. (2009). How barn owls (*Tyto alba*) visually follow moving voles (*Microtus socialis*) before attacking them. *Physiology & Behavior*, *98*(3), 359–366. https://doi.org/10.1016/j.physbeh.2009.06.016

Grood, E. S., & Suntay, W. J. (1983). A joint coordinate system for the clinical description of three-dimensional motions: Application to the knee. *Journal of Biomechanical Engineering*, *105*(2), 136–144. https://doi.org/10.1115/1.3138397

Grytsyshina, E. E., Kuznetsov, A. N., & Panyutina, A. A. (2016). Kinematic constituents of the extreme head turn of *Strix aluco* estimated by means of CT-scanning. *Doklady Biological Sciences*, *466*(1), 24–27. https://doi.org/10.1134/S0012496616010087

Kambic, R. E., Biewener, A. A., & Pierce, S. E. (2017). Experimental determination of three-dimensional cervical joint mobility in the avian neck. *Frontiers in Zoology*, *14*(1), 37. https://doi.org/10.1186/s12983-017-0223-z

De Kok-Mercado, F., Habib, M., Phelps, T., Gregg, L., & Gailloud, P. (2013). Adaptations of the owl's cervical & cephalic arteries in relation to extreme neck rotation. *Science*, *339*(6119), 514. https://doi.org/10.1126/science.339.6119.514

Krings, M., Nyakatura, J. A., Boumans, M. L. L. M., Fischer, M. S., & Wagner, H. (2017). Barn owls maximize head rotations by a combination of yawing and rolling in functionally diverse regions of the neck. *Journal of Anatomy*, *231*(1), 12–22. https://doi.org/10.1111/joa.12616

Krings, M., Nyakatura, J. A., Fischer, M. S., & Wagner, H. (2014). The cervical spine of the American barn owl (*Tyto furcata pratincola*): I. Anatomy of the vertebrae and regionalization in their S-shaped arrangement. *PLoS ONE*, *9*(3), e91653. https://doi.org/10.1371/journal.pone.0091653

Kuroda, N. (1962). On the cervical muscles of birds. *Journal of the Yamashina Institute for Ornithology*, *3*(3), 189–211. https://doi.org/10.3312/jyio1952.3.189

Landolt, R., Vanden Berge, J. C., & Zweers, G. A. (1989). The cervical column of mallard and chicken. *Fortschritte der Zoologie*, *35*, 74–78.

Landolt, R., & Zweers, G. (1984).). Anatomy of the muscle-bone apparatus of the cervical system in the mallard (*Anas platyrhynchos* L.). *Netherlands Journal of Zoology*, *35*(4), 611–670. https://doi.org/10.1163/002829685X00226

van der Leeuw, A. H. J. (1991). Scaling effects on cervical kinematics in drinking Anatidae. *Netherlands Journal of Zoology*, *42*(1), 23–59. https://doi.org/10.1163/156854292X00026

van der Leeuw, A. H. J., Bout, R. G., & Zweers, G. A. (2001a). Control of the cranio-cervical system during feeding in birds. *American Zoologist*, *41*(6), 1352–1363. https://doi.org/10.1093/icb/41.6.1352

van der Leeuw, A. H. J., Bout, R. G., & Zweers, G. A. (2001b). Evolutionary morphology of the neck system in ratites, fowl and waterfowl. *Netherlands Journal of Zoology*, *51*(2), 243–262. https://doi.org/10.1163/156854201X00297

Morgan, D. L. (1990). New insights into the behavior of muscle during active lengthening. *Biophysical Journal*, *57*(2), 209–221. https://doi.org/10.1016/S0006-3495(90)82524-8

Ohayon, S., van der Willigen, R. F., Wagner, H., Katsman, I., & Rivlin, E. (2006). On the barn owl's visual pre-attack behavior: I. Structure of head movements and motion patterns. *Journal of Comparative Physiology A*, *192*(9), 927–940. https://doi.org/10.1007/s00359-006-0130-9

Steinbach, M. J., & Money, K. E. (1973). Eye movements of the owl. *Vision Research*, *13*(4), 889–891. https://doi.org/10.1016/0042-6989(73)90055-2

Walls, G. L. (1963). *The vertebrate eye and its adaptive radiation*. Hafner Publishing Company.

Weijs, W. A., & van der Wielen-Drent, T. K. (1983). The relationship between sarcomere length and activation pattern in the rabbit masseter muscle. *Archives of Oral Biology*, *28*(4), 307–315. https://doi.org/10.1016/0003-9969(83)90073-0

Wu, G., Van Der Helm, F. C. T., (DirkJan) Veeger, H. E. J., Makhsous, M., Van Roy, P., Anglin, C., Nagels, J., Karduna, A. R., McQuade, K., Wang, X., Werner, F. W., & Buchholz, B. (2005). ISB recommendation on definitions of joint coordinate systems of various joints for the reporting of human joint motion – Part II: Shoulder, elbow, wrist and hand. *Journal of Biomechanics*, *38*(5), 981–992. https://doi.org/10.1016/j.jbiomech.2004.05.042

Wu, G., Siegler, S., Allard, P., Kirtley, C., Leardini, A., Rosenbaum, D., Whittle, M., D'Lima, D. D., Cristofolini, L., Witte, H., Schmid, O., & Stokes, I. (2002). ISB recommendation on definitions of joint coordinate system of various joints for the reporting of human joint motion—Part I: Ankle, hip, and spine. *Journal of Biomechanics*, *35*(4), 543–548. https://doi.org/10.1016/S0021-9290(01)00222-6

Zarnik, B. (1926). On the ethology of plesiosaurs with contributions to the mechanism of the cervical vertebrae of recent sauropsids. *Societas Scientiarum Naturalium Croatica*, *37–38*, 424–479.

Zusi, R. L., & Storer, R. W. (1969). Osteology and rnyology of the head and neck of the Pied-billed grebes (*Podilyrnbus*). *Miscellaneous Publications Museum of Zoology, University of Michigan*, *139*, 1–49.

Zweers, G., Bout, R., & Heidweiller, J. (1994). Motor organization of the avian head-neck system. In M. N. O. Davies & P. R. Green (Eds.), Perception and motor control in birds (pp. 201–221). Springer. https://doi.org/10.1007/978-3-642-75869-0_12

Zweers, G. A., Vanden Berge, J. C., & Koppendraier, R. (1987). Avian cranio-cervical systems. Part I: Anatomy of the cervical column in the chicken (*Gallus gallus* L.). *Acta Morphologica Neerlando-Scandinavica*, *25*(3), 131–155.

SUPPORTING INFORMATION

Additional supporting information can be found online in the Supporting Information section at the end of this article.

How to cite this article: Panyutina, A. A., & Kuznetsov, A. N. (2023). Are owls technically capable of making a full head turn? *Journal of Morphology*, *285*, e21669. https://doi.org/10.1002/jmor.21669